Structural insights into cobalamin loading and reactivation of human methionine synthase

Douglas S. M. Ferreira[1,2], Katie McLennan[2], Calum Diamond[2], Melanie Vollmar[3,5], Wasim Kiyani[3], D. Sean Froese[3,6], Jola Kopec[3], Henry J. Bailey[3,7], Rod Chalk[1], Arnaud Baslé[2], Jonathan M. Elkins[1], Jesse A Coker[4], Wyatt W. Yue[1,2,3]*, Thomas J. McCorvie[2]*

[1]Centre for Medicines Discovery, Nuffield Department of Clinical Medicine, University of Oxford, Oxford, OX3 7DQ, UK
[2]Biosciences Institute, The Medical School, Newcastle University, Newcastle upon Tyne, NE2 4HH, UK
[3]Structural Genomics Consortium, University of Oxford, Oxford, OX3 7DQ, UK
[4]Center for Therapeutics Discovery, Lerner Research Institute, Cleveland Clinic, Cleveland, Ohio, 44195, United States.
[5]Present address: European Bioinformatics Institute (EMBL-EBI), Main Building, A2-34, Wellcome Genome Campus, Hinxton, CB10 1SD, United Kingdom
[6]Present address: Division of Metabolism and Children's Research Center, University Children's Hospital Zurich, University of Zurich, Zurich 8008, Switzerland
[7]Present address: Institute of Biochemistry II, Medical Faculty, Goethe-University, Frankfurt am Main and Buchmann Institute for Molecular Life Sciences, Frankfurt am Main, Germany

*Correspondence e-mail: wyatt.yue@newcastle.ac.uk; thomas.mccorvie@newcastle.ac.uk

Human methionine synthase (MTR) is an essential enzyme of one carbon metabolism. Consisting of a catalytic N-half and a cobalamin binding C-half, MTR utilises this intricate organometallic cofactor in the methyl transfer from methyltetrahydrofolate to homocysteine producing methionine. Cobalamin loading into MTR, and its subsequent activation, requires methylmalonic aciduria and homocystinuria Type D (MMADHC) protein and methionine synthase reductase (MTRR), respectively. However, the molecular basis of cobalamin binding and activation of human MTR aided by MMADHC and MTRR remains unknown. Here, using cryo-electron microscopy, we determined structures of human MTR in its apo, and cobalamin bound states. Apo MTR adopts a conformation where the two halves of the enzyme act independently with the C-half posed to bind cobalamin. Binding of cobalamin and its activation causes conformational changes in MTR that result in a flexible catalytically active state. AlphaFold predictions, validated by interaction studies, show that MMADHC interacts with the C-half of apo MTR to facilitate cobalamin loading. Unexpectedly we found that MTRR interacts at two distinct sites within the C-half of MTR which may aid in activation. Collectively these findings lay the groundwork to uncover the mechanisms through how MMADHC and MTRR coordinate cobalamin loading and activation of human MTR.

Introduction

Methionine synthase (EC 2.1.1.13; 5-methyltetrahydrofolate-homocysteine methyltransferase, MTR) forms a crucial node connecting the methionine and folate cycles in one-carbon metabolism. MTR catalyses the methylation of homocysteine (Hcy) using 5-methyltetrahydrofolate (MeTHF) as the methyl group donor, to generate methionine (Met) and tetrahydrofolate (THF)[1]. A key function of MTR is to ensure a supply of Met precursor to synthesise the global methyl donor *S*-adenosyl-L-methionine (SAM) involved in a myriad of epigenetic methylation reactions[2]. MTR also serves as an important regulator of the folate cycle which carries one-carbon units for purine and pyrimidine biosynthesis[3,4]. In humans, the primary circulating folate species is MeTHF[5], and MTR is the only enzyme that can metabolise MeTHF to regenerate THF, the active form required for subsequent one-carbon transfer reactions and DNA synthesis[6].

MTR is a ~140 kDa monomeric protein comprising a catalytic N-half and a cofactor binding C-half (Fig. 1a). The N-half consists of two rigidly linked (Linker 1) TIM barrels, known as a homocysteine (Hcy) domain and a folate (Fol) domain, which exclusively bind the substrates Hcy and MeTHF, respectively. Connected to the N-half by a flexible linker (Linker 2), the C-half consists of a four-helical bundle Cap domain, a cobalamin binding domain (Cob), and a SAM binding activation domain (Act)[7]. Notably, MTR is one of only two human enzymes that uses cobalamin (Cbl) as a cofactor[7].

Cbl, also known as vitamin B_{12}, is a large 1.3 kDa molecule consisting of a centrally bound hexacoordinated cobalt ion within a corrin ring, a ribose group tethered 5,6-dimethyl-benzimidazole (DMB) tail that can coordinate as a lower α-axial ligand ('base-on') and an upper β-axial ligand. This upper ligand can vary with the most common being a cyano or hydroxy group, whereas adenosyl or methyl group are the biological active forms in humans[7]. Within MTR the Cbl cofactor binds with the DMB group disengaged ('base-off') where in some instances a conserved histidine residue can bind as the lower axial ligand (His-off or His-on). During MTR's catalytic cycle, the bound Cbl undergoes different cobalt oxidation and coordination states, such as alternating between the oxidised hexacoordinated methylcob(III)alamin form and the reduced tetracoordinated cob(I)alamin form. Cob(I)alamin is a strong nucleophile capable of extracting the methyl group from MeTHF, however it is also highly susceptible to oxidative inactivation, resulting in a cob(II)alamin form that renders MTR inactive. This necessitates the enzyme to enter a reactivation cycle where a reductive methylation process regenerates the functional methyl(III)cobalamin form from the inactive cob(II)alamin[8]. Previous structural studies using isolated domains of the bacterial orthologue, MetH, have suggested that for MTR to function large conformational changes are required in order for the Cob domain to interact with the Hcy and Fol domains within the rigid N-half during catalysis but also with the Act domain in the C-half during reactivation[9-11].

Differentiating from its bacterial counterpart, human MTR has been shown to interact with three eukaryote-only proteins, namely methylmalonic aciduria and homocystinuria type C protein (MMACHC), methylmalonic aciduria and homocystinuria type D protein (MMADHC), and methionine synthase reductase (MTRR)[12]. MMACHC and MMADHC are known Cbl processing enzymes where MMACHC has Cbl reductase and dealkylase activities, to process various Cbl forms by removing the upper axial ligand to eventually produce cob(II)alamin[13]. Recent studies have shown that MMADHC can form a complex with MMACHC[14,15], and can load Cbl onto MTR through forming a rare cobalt-sulfur bond donating a cysteine residue as one of the axial ligands[16,17]. MTRR is a multi-domain diflavin oxidoreductase that contains at its N-terminus a flavin mononucleotide (FMN) binding domain, flexibly linked to a C-terminal module that contains of a connecting (Conn) domain, a flavin adenine dinucleotide (FAD) binding domain, and a nicotinamide adenine dinucleotide phosphate (NADPH) binding domain[18]. MTRR plays a key role in reactivating MTR for catalysis, working in concert with the SAM-bound Act domain of MTR. MTRR donates electrons from NADPH to reduce and methylate the inactive cob(II)alamin bound to MTR, to produce functional methylcob(III)alamin[19,20]. This is a multistep sequential process where electrons from NADPH are initially transferred to FAD and then FMN before ultimately being transferred to the bound

Cbl[7]. In bacteria this function is carried out by two separate proteins, flavodoxin and flavodoxin reductase[21]. Significantly, the essential roles of MTR and its interaction partners in human health are stressed by reported pathogenic mutations in their corresponding genes, that are associated with a collection of rare inherited metabolic disorders[22]. Altered Cbl and folate metabolism is also known to be linked to an increased risk of neural tube defects[23].

Little is known on how human MTR binds Cbl and if it shares the same conformational flexibility as its bacterial orthologues. Even less is known on how human MTR interacts with its eukaryote specific partner proteins that support its functionality. To address these questions, we have used cryo-electron microscopy (cryo-EM) together with AlphaFold 3 (AF3) structure predictions, to investigate how human MTR binds Cbl and how it interacts with its functional protein partners MMACHC, MMADHC, and MTRR.

Results

Human MTR can be purified without bound cobalamin

We expressed and purified apo full-length human MTR (MTR^{FL}) with a C-terminal His_6 and FLAG tag from insect cells. Though milligrams of recombinant protein could be obtained, size-exclusion gel filtration demonstrated that the majority of MTR^{FL} formed aggregates with some monomeric protein (Supplementary Fig.1a). Negative stain electron microscopy (NS-EM) confirmed the presence of homogenous and monodisperse particles from the monomeric peak (Supplementary Fig. 1b). The molecular weight was determined to be 142.69 kDa by native mass-spectrometry, agreeing with the calculated molecular weight of 143.85 kDa (with tag) and confirming the purified monomeric protein was in the apo form without any detectable bound Cbl ligands (Supplementary Fig.1c) as previously reported[24,25].

Using an absorbance-based activity assay[26] monomeric MTR^{FL} was determined to be catalytically active (Supplementary Fig. 1d). To further assess functionality, we turned to thermal shift experiments testing MTR^{FL} along with purified $MTR^{N\text{-}Half}$ (Hcy and Fol domains) and $MTR^{C\text{-}Half}$ (Cap, Cob, and Act domains) constructs. Here we determined the melting temperature (T_m) of these constructs as purified along with being in the presence of relevant substrates and different cobalamins. In these experiments, MTR^{FL} was stabilised by MeTHF with a 3.3 ± 0.3 ºC melting temperature increase (ΔT_m) (Supplementary Fig. 1e, g). MeTHF also induced a ΔT_m increase of 4.8 ± 0.4 °C for $MTR^{N\text{-}Half}$, whereas no statistically significant change in T_m was observed for $MTR^{C\text{-}Half}$ as expected (Supplementary Fig.1e, g). In contrast, both Hcy and SAM showed no T_m changes for any of the three constructs (Supplementary Fig. 1g). We then tested hydroxycobalamin (HOCbl), cyanocobalamin (CNCbl), and methylcobalamin (MeCbl) against the three constructs. As expected, no T_m changes were observed for $MTR^{N\text{-}Half}$, whereas all three Cbl ligands stabilised both MTR^{FL} and $MTR^{C\text{-}Half}$ with MeCbl eliciting the largest T_m shifts (Supplementary Fig. 1f, g). Overall, these experiments demonstrate that we can successfully purify functional apo full-length and constructs corresponding to each half of human MTR.

Apo MTR is in a reactivation conformation for cobalamin loading

Having successfully purified apo MTR^{FL} and encouraged by our NS-EM results, we attempted to determine a high-resolution structure of this as-purified, Cbl free state by cryo-EM. Initial screening resulted in 2D classes representing only the C-half of MTR likely in the reactivation state where the Act domain is engaged with the Cob domain (Supplementary Fig. 2a). Unfortunately, after many attempts we could not produce conditions that yielded reliable good 2D classes representing the entirety of full-length MTR, likely due to instability and air-water denaturation. To overcome this, we screened and collected data in the presence of MeTHF, reasoning that it would stabilise MTR^{FL} as found in our thermal shift experiments (Supplementary Fig 1e, g). Initial screening resulted in separate 2D classes of both halves of MTR (Supplementary Fig. 2b). Despite multiple processing strategies no classes showed the concurrent presence of both halves of MTR. A larger dataset was then collected which allowed us to determine a 3.1 Å resolution structure of the 70 kDa N-half bound to MeTHF and a 2.8 Å resolution structure of the 68 kDa apo C-half (Fig. 1, Supplementary Fig. 3, 9, 10).

The N-half structure of MTR^{FL} confirmed that the Hcy and Fol domains are TIM barrel folds with the short Linker 1 (Pro347 to Phe371) that tightly locks the domains side by side (Fig. 1b). This arrangement implies that large conformational changes are required for the Cob domain to interact with the N-half domains during catalysis as has been suggested for bacterial MetH[7,9]. The Hcy domain showed weak density for a disulfide bond between Cys260 and Cys323 with no other apparent density for substrate (Fig 1b, Supplementary Fig. 4a). On the other hand, the Fol domain showed clear density for the MeTHF ligand (Fig. 1c) making interactions with the conserved residues Asn470, Asp537, and Asn579 through its pterin ring containing the methyl group. Additionally, the p-aminobenzoic acid (PABA) side chain of MeTHF forms hydrogen bonds with the residues Arg384, Arg585, and Arg591 (Fig. 1c). This MeTHF bound structure is highly similar to our previously deposited 2.7 Å crystal structure of the $MTR^{N\text{-}Half}$ construct alone bound to THF (PDB 4CCZ), showing that the binding of MeTHF is near identical to THF, with a RMSD of 0.68 Å (Supplementary Fig. 4a). Comparing our human N-half cryo-EM structure to the reported N-half sections from *Thermus filiformis* (PDB 8G3H) and *Thermus thermophilus* HB8 (PDB 8SSC) MetH structures demonstrates how this tight arrangement between the Hcy and THF domains is evolutionarily conserved (Supplementary Fig. 4b)[24,27].

The Cbl free C-half structure of MTR^{FL} was found to be in a conformation where the Cap domain is displaced (Cap-off) from the Cob domain, allowing free access to the Cbl binding pocket and engagement with the Act domain (Fig. 1d). No density was apparent for the Cbl cofactor as expected (Fig. 1e). This domain arrangement is similar to that reported in crystal structures of the isolated C-half from bacteria MetH bound to cob(II)alamin, which has been suggested to be the reactivation conformation productive for reductive methylation[10,28,29] (Supplementary Fig. 4c). Structural alignment against the *Escherichia coli* C-half structure bound to cob(II)alamin (PDB 3BUL) and the apo C-half section from *T. thermophilus* (PDB 8SSC) shows only minor differences in the relative position of the Cap to the other domains (Supplementary Fig. 4c). The expected lower axial ligand for the Cbl cofactor, His785, is in a His-off conformation and the corresponding histidine sidechain adopts variable positions in the bacteria MetH structures of the His-off state (Fig 1e, Supplementary Fig. 4c). Tyr1177, which promotes the tetracoordinated cob(I)alamin form during MTR reactivation[29], is positioned 3.7 Å closer to the putative position of the cobalt atom, when compared to the *apo* MeTH structure from *T. thermophilus* (Supplementary Fig. 4c)[24].

183

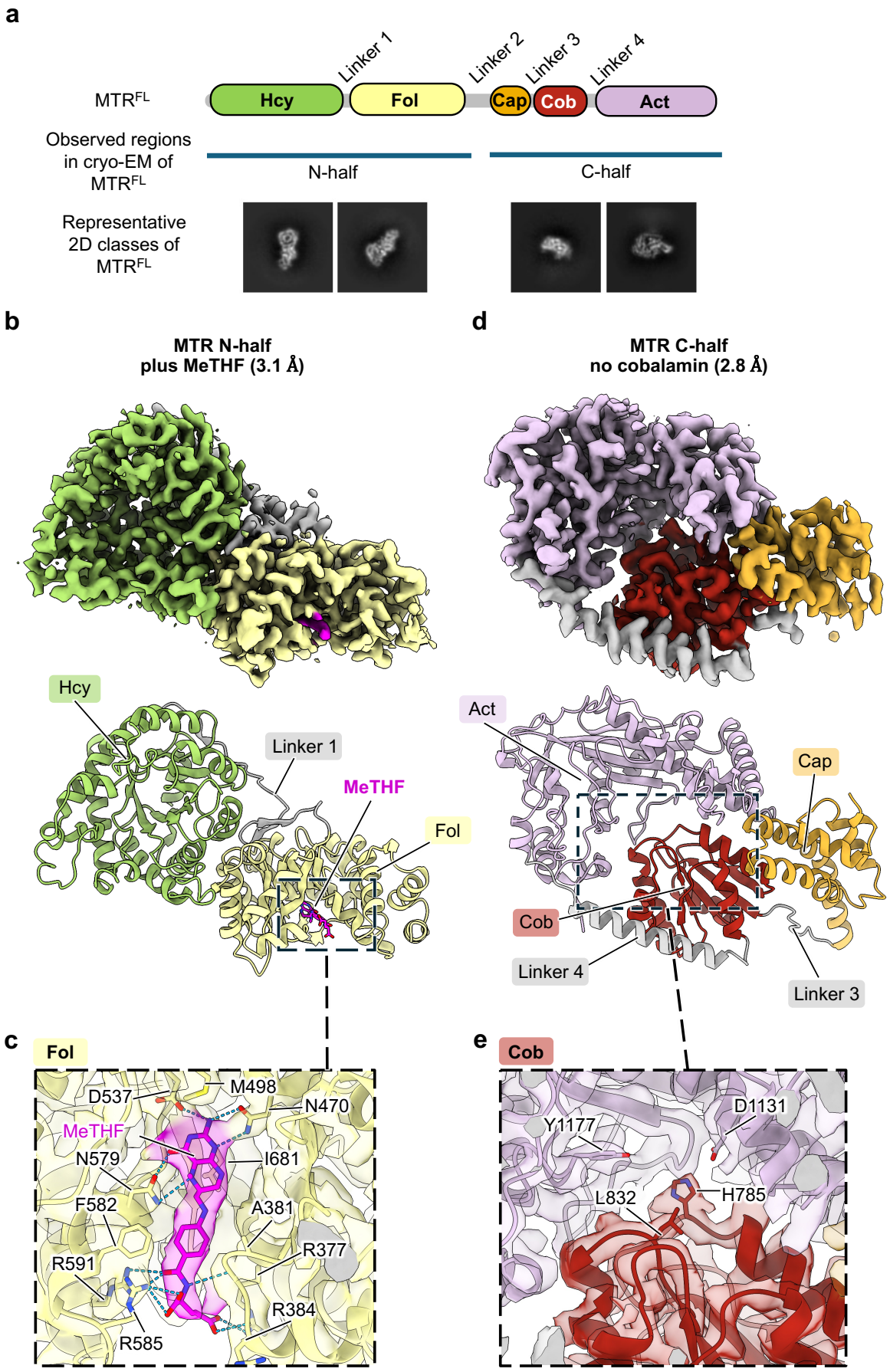
a
MTR^FL
Hcy
Fol
Cap
Cob
Act
Linker 1
Linker 2
Linker 3
Linker 4
Observed regions in cryo-EM of MTR^FL
N-half
C-half
Representative 2D classes of MTR^FL
b
MTR N-half plus MeTHF (3.1 Å)
Hcy
Linker 1
MeTHF
Fol
d
MTR C-half no cobalamin (2.8 Å)
Act
Cap
Cob
Linker 4
Linker 3
c
Fol
D537
M498
N470
MeTHF
N579
I681
F582
A381
R377
R591
R384
R585
e
Cob
Y1177
D1131
L832
H785

184

Fig. 1 | Cryo-EM analysis of MTR^{FL} bound to MeTHF. a, Cartoon schematic of the domain organization of MTR. Regions resolved of MTR^{FL} by cryo-EM are indicated. Representative 2D classes for each MTR map show the presence of just one half of the full-length enzyme. **b**, The 3.1 Å resolution map and model of N-half bound to MeTHF. Domains are coloured as in Fig. 1a and MeTHF is coloured magenta. **c,** Overlay of the map and model of the MeTHF binding pocket in the N-half of MTR^{FL}, highlighting key residues and the ligand. **d,** The 2.8 Å resolution map and model of the C-half with no bound Cbl cofactor. Domains are coloured as in Fig. 1a. **e,** Overlay of the map and model of the cobalamin binding pocket in the C-half of MTR^{FL}, highlighting key residues in the region and showing no detectable density corresponding to Cbl.

Binding of HOCbl to MTR causes local structural changes

The conformation of the C-half of MTR^{FL} suggests that the apo enzyme forms this "reactivation-like" conformation before the binding of free Cbl from solution or Cbl loading assisted by MMADHC. Therefore, to determine the conformational changes upon initial binding of Cbl, we collected cryo-EM data of MTR^{FL} in the presence of MeTHF and HOCbl. SAM was also added in an attempt to determine what conformational changes could occur before methylation of the bound Cbl. As with the MeTHF dataset, only separate 2D classes of the N-half and C-half alone could be determined, suggesting their independence when MTR^{FL} is in the presence of these ligands. Processing of the N-half particles generated a 2.9 Å resolution structure (Supplementary Fig. 5, 9, 10), identical to that with MeTHF alone (RMSD 0.356 Å) (Supplementary Fig. 6a).

Processing of the C-half particles revealed two states with an overall conformation as the Cbl free form (Supplementary Fig. 5, 9, 10). Inspection of the Cob domain in both states showed clear density for the bound cofactor, HOCbl (Fig. 2a, b, Supplementary Fig. 6b); however, the density for SAM in the Act domain was discontinuous and did not allow for modelling, suggesting flexibility or low occupancy of this ligand (Supplementary Fig. 6c). The first state, determined to a resolution of 2.9 Å, is representative of the majority of the C-half particles. In this state, density was apparent for HOCbl bound in a Cbl(II), base-off, His-off state (Fig. 2a, Supplementary Fig. 6b). Density for the dimethylbenzimidazole (DMB) tail bound in the pocket of the Cob domain was clear, interacting with conserved residues Ser830 and Gly860 (Supplementary Fig. 6b). The corrin ring showed less apparent density, suggesting flexibility with Leu832 in the location of the lower axial ligand (Fig. 2c, Supplementary Fig. 6b).

The second state was determined to a resolution of 3.2 Å (Fig. 2b, Supplementary Fig. 6b) and is representative of the minority of the particles. Similar to the His-off state described above, density was apparent for HOCbl, however its corrin ring has shifted by 2.8 Å (Fig. 2c, d) and is now in a His-on state, where His785 becomes the lower axial ligand (Fig. 2c). Furthermore, conformational changes are apparent in the Cob domain when comparing the His-off and His-on structures (Fig. 2d). These changes occur throughout the entire Cob domain, involving a shift away from the Act domain during the transition from the His-off to the His-on state. The density of the helical Linker 4 between the Cob and Act domains is also less defined (Fig. 2b), suggesting a degree of flexibility in this state.

In the C-half maps of both states, the Cap domain showed less detail than the other domains, suggesting heterogeneity possibly due to flexibility. Interested in analysing this further, we turned to 3D variability analysis (3DVA)[30] where we compared the apo C-half map against the Cbl bound C-half map with both His-off and His-on particles pooled together (Supplementary Fig. 7, Supplementary Movies 1-4). For both the apo and Cbl bound states, flexing of the Cap domain was evident where it moves towards the Act domain. Simultaneously, the Cob domain appears to be moving away from the Act domain (Supplementary Fig. 7a, b, Supplementary Movies 1, 3). Other movements were observed in the Cbl bound state where the Cbl cofactor transitions from His-off to His-on correlating with larger movements of the Cob domain away from the Act domain (Supplementary Fig. 7b, Supplementary Movie 3) along with some rotation towards the Cap (Supplementary Fig. 7d,

Supplementary Movie 4). We believe that this displacement of the Cob domain is representative of the conformational changes that occur when MeCbl is formed via reductive methylation and the subsequent change from a five-coordinate His-off Cap-off state to a six-coordinate His-on Cap-on state[31]. As no electron source was added to our sample, reductive methylation cannot occur, thereby allowing us to trap a small percentage of the MTR protein bound to HOCbl in this putative prelude state (His-on, Cap-off) before entering the catalytic cycle, similar to what has been suggested for a crystal structure of the His-on HOCbl bound state of the C-half from E. *coli* (PDB 3IV9)[29].

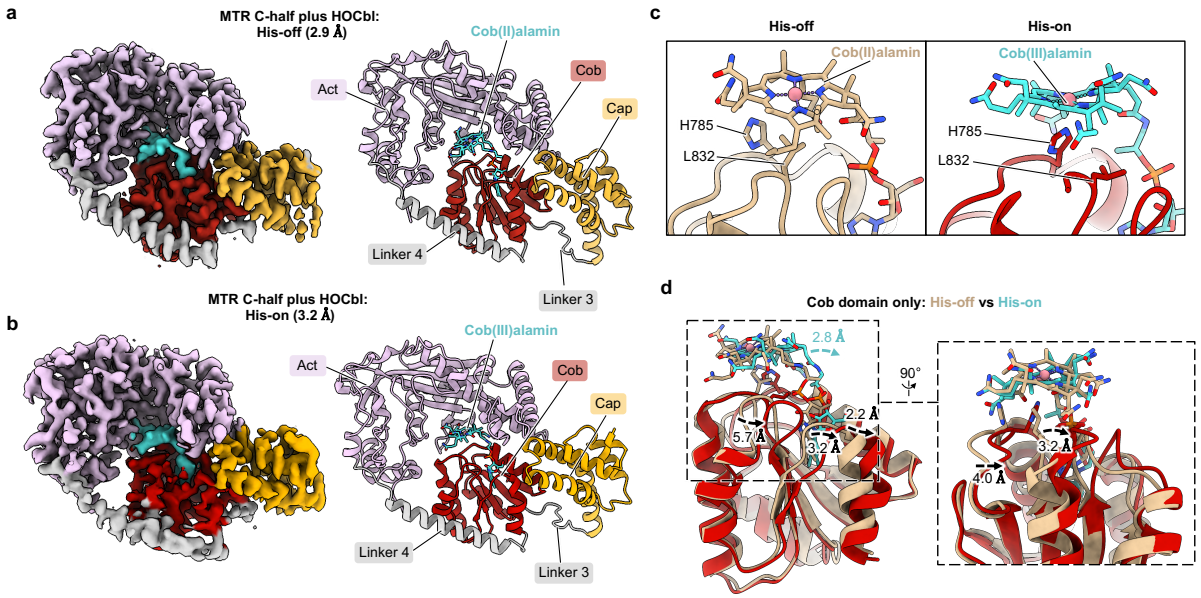

Fig. 2 | Cryo-EM analysis of the C-half of MTR^{FL} bound to HOCbl. a, The 2.9 Å resolution map and model of the C-half of MTR^{FL} bound to HOCbl in a His-off state. Domains are coloured as in Fig. 1a and HOCbl is coloured cyan. **b,** The 3.2 Å resolution map and model of the C-half of MTR^{FL} bound to HOCbl in a His-on state. Domains are coloured as in Fig. 1a and HOCbl is coloured cyan. **c,** Positioning of HOCbl and His785 in the His-off state (left, beige) and His-on state (right, cyan). **d,** Comparison of the movements of HOCbl and the Cob domain between the His-off and His-on states. The HOCbl and Cob domain in the His-off state are shown in beige, while HOCbl in the His-on state is shown in cyan, and the Cob domain in the His-on state is shown in red.

Binding of MeCbl remodels the C-half of MTR^{FL}

After Cbl loading and reductive methylation aided by MTRR, MTR is activated and transforms into a six-coordinate His-on MeCbl-bound conformation, poised to begin the catalytic cycle[32]. Recent studies have suggested that *T. filiformis* and *T. thermophilus* MetH enters a so-called “resting” or “gating” state in the presence of Cbl and without substrates. In this state the N-half (Hcy and Fol domains) stably interacts with the Cap and Cob domains of the C-half in a Cap-on and a disengaged Act domain conformation[27,33]. Interested in capturing a similar Cap-on state of human MTR without substrate, we prepared MTR^{FL} in the presence of MeCbl for cryo-EM analysis. MeCbl has been shown to readily bind to the Cob domain from solution[17] and also stabilised the protein in our thermal shift experiments (Supplementary Fig. 1e, g).

Preliminary screening of MTR^{FL} in the presence of MeCbl resulted in discernible 2D classes of the 70 kDa N-half only, and unlike in our previous datasets no apparent 2D classes could be determined corresponding to the C-half. However, as this sample of MTR^{FL} lacked any substrates, a larger dataset was then collected that resulted in a 2.7 Å resolution structure of the apo N-half of MTR^{FL} (Fig. 3b, Supplementary Fig. 8-10). Comparing this structure with our MeTHF- and THF-bound structures shows little conformational changes in both Hcy and

Fol domains (Fig. 3c). No other domains were present in the map, and despite further processing no other states containing the N-half could be found unlike what has been reported for structures of thermophilic MTR homologues[27,33]. In these structures a loop located in the Fol domain changes conformation due to the absence of folate, and was suggested to play a role in altering the conformation of Linker 2 which connects the two halves of the enzyme, resulting in the "resting/gating" state[27,33]. However, unlike thermophilic MetH, the folate sensing loop in human MTR (residues 613-619) shows no structural changes due to the absence of folate and is positioned in a similar manner as the ligand bound states (Fig. 3d).

The lack of a C-half structure from this dataset could have been due to a combination of intrinsic flexibility and air-water denaturation. In theory the binding of MeCbl should induce large conformational changes in the C-half, shifting MTR into a catalytical competent state and displacing the Act domain from the Cob domain to allow interactions of the bound Cbl with the N-half domains and Cap during catalysis. Further careful processing of our MeCbl-bound dataset revealed classes equating to the Act domain of MTR^{FL} (≈ 38 kDa), showing its disengagement from the Cob domain (Fig. 3e). Despite its small size, further processing resulted in a 3.1 Å resolution map (Fig. 3e, Supplementary Fig. 8-10). Comparison of this Act domain-alone structure with the Act domain in the context of our C-half structures (i.e. together with Cob and Cap domains) shows little structural changes within the Act domain (Supplementary Fig. 11a). Comparison to the crystal structure of an isolated Act domain construct (PDB 2O2K)[34] showed that only a few residues in flexible regions displayed any significant conformational differences, likely resulting from crystal packing (Supplementary Fig. 11b). Therefore, we interpret that our MeCbl-bound MTR^{FL} dataset is likely in a His-on, Cap-on state consisting of three flexible independent modules, namely the N-half (≈ 70 kDa), the Cap and Cob domains (≈ 28 kDa), and the Act domain (≈ 38 kDa). Despite considerable effort in data processing, we failed to find any 2D classes equating to the MeCbl bound Cap-Cob domains, likely due to its small size and its position between the N-half and Act domain. Indeed, inspecting the 2D classes and low pass filtering our Act domain map show the presence of blurry low-resolution density at the expected location of these two domains, suggesting their presence (Supplementary Fig. 11c, d). Although the difference between our MeCbl-bound structure and the reported structures of thermophilic MetH bound to inactive Cbl[27,33] forms may be due to variations in sample preparation, it suggests that MTR can adopt more conformations than has been previously suggested (Fig. 3f).

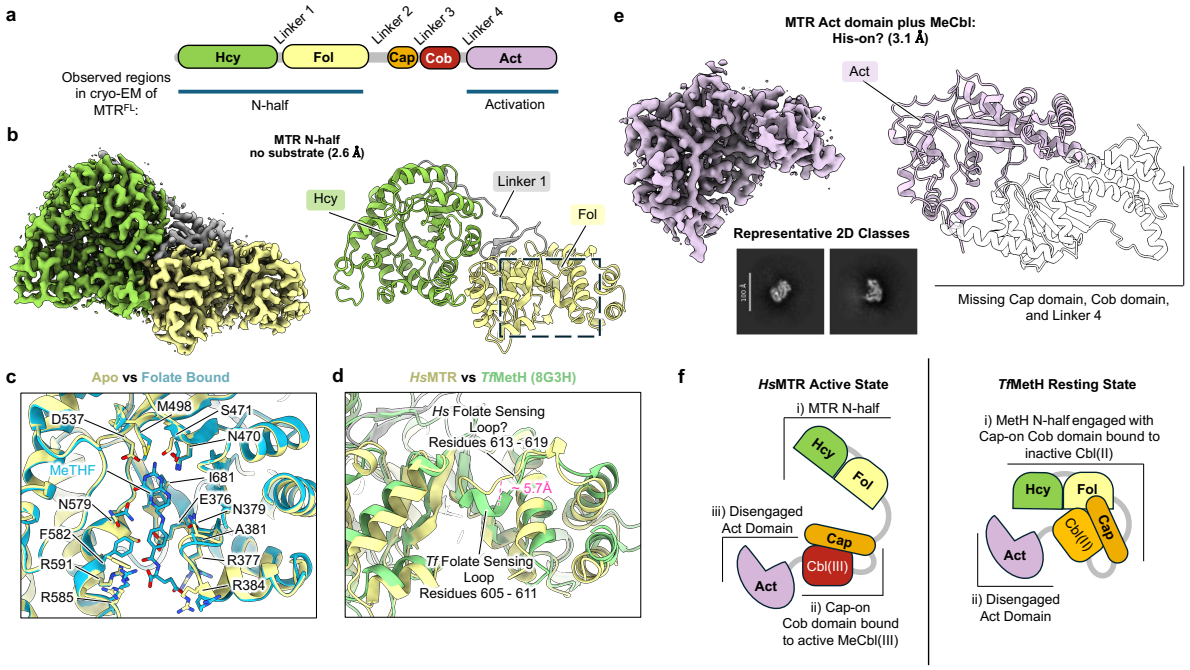

Fig. 3 | Cryo-EM analysis of MTR bound to MeCbl. a, Cartoon schematic of the domain organization of MTR. Domains resolved by cryo-EM are indicated. **b,** The 2.6 Å resolution map and model of the N-half of MTR^{FL} in the apo state. Domains are coloured as in Fig. 3a. **c,** Structural alignment of our apo (yellow) and folate bound (cyan) structures focused on the folate binding site. Little conformational changes occur due to folate binding with only a slight shift away from the active site for the small loop containing Ala381. **d,** Structural alignment of our apo N-half structure (yellow) and thermophilic MetH structure (8G3H, light green) focused on the folate binding site. Unlike the position of residues 605-611 in thermophilic MetH, corresponding to a putative folate sensing loop, no structural changes occur in residues 613-619 in human MTR due to the absence of folate. **e,** The 3.1 Å resolution map and model of the MTR^{FL} Act domain. The 2D classes shown are representative of the Act domain as observed in the cryo-EM data analysis. In the model the missing linkers, Cap, and Cob domains are also shown as a transparent model arranged as found in our C-half structures. **f,** Proposed domain arrangements as cartoon representations of MeCbl-bound active human MTR and thermophilic HOCbl-bound inactive MetH, without substrate. In human MTR MeCbl binding results in a conformation with the N-half, Cap-Cob domains, and Act domain acting as three independent modules. In contrast, HOCbl binding to thermophilic MetH results in a two-module conformation with the N-half plus Cap-Cob domains, and the Act domain acting independently.

MMADHC, not MMACHC, binds MTR directly to load cobalamin

The cobalamin chaperone enzymes MMACHC and MMADHC can form a heterodimer in the presence of Cbl[14], and previous studies have implied a stable complex of MTR with MMACHC and MMADHC[12,35]. Additionally, Cbl transfer from MMADHC to MTR has been monitored through size-exclusion chromatography[17]. However, no structural insights into their complex formation have been determined experimentally. Therefore, we turned to AlphaFold3 (AF3)[36] modelling to predict how both MMACHC and MMADHC could interact with MTR to load Cbl.

AF3 predicted modelling of the MTR binary complexes was initially carried out using the sequences of the full-length proteins. This was then followed by using only the sequences of the N- and C-halves of MTR to confirm which domains were involved in protein-protein interactions. AF3 models for the MTR^{FL}-$MMACHC^{FL}$, $MTR^{N\text{-}Half}$-$MMACHC^{FL}$, and $MTR^{C\text{-}Half}$-$MMACHC^{FL}$ complexes demonstrated random spatial positions of MMACHC on MTR (Supplementary Fig 12, 14a, b). This combined with their low ipTM scores[36] (~ 0.2), which is a confidence measure of the accuracy of predicted complexes, suggest that MMACHC may not form a complex with MTR. In contrast the AF3 models for the MTR^{FL}-$MMADHC^{FL}$ complex (Fig. 4a, Supplementary Fig. 13) and the $MTR^{C\text{-}Half}$-$MMADHC^{FL}$ subcomplex (Fig. 4b, Supplementary Fig. 14d) resulted in highly similar and consistent predicted models with correspondingly moderate to high ipTM scores[36] above 0.5. On the other hand, the $MTR^{N\text{-}Half}$-$MMADHC^{FL}$ subcomplex showed random spatial positions of each protein with a corresponding low ipTM score suggesting that MMADHC does not interact with either the Hcy or Fol domains of MTR (Supplementary Fig. 14c).

In both sets of predictions with either MTR^{FL} or $MTR^{C\text{-}Half}$, MMADHC is straddled above the Cob domain of MTR in the reactivation conformation, forming potential interactions with all three domains of the C-half of MTR (Fig. 4a, b, Supplementary Fig. 13, 14a, b). This interface results in the loop aa 255-266 from MMADHC to point towards the Cbl-binding pocket in the Cob domain of MTR. This loop harbours the residues Cys261 and Cys262, which are responsible for the binding of Cbl and its loading into MTR[17]. Superimposing the predicted models with our HOCbl-bound C-half structure of MTR^{FL} and the crystal structure of MMADHC coordinating a thiolato-cobalamin ligand (PDB 6X8Z)[37] suggests that some conformational changes are required for Cbl loading. The Cbl cofactor needs to move 4.3 Å towards the binding pocket within the Cob domain of MTR when being loaded by MMADHC (Supplementary Fig 15).

To verify MTR's predicted lack of interaction with MMACHC and its predicted positive interaction with MMADHC we performed affinity-based pulldowns using MTR^{FL} against a GST

fusion of MMADHC$^{\Delta N}$ (MMADHC lacking the first 123 residues that were predicted to be disordered) and a GST fusion of full-length MMACHC (Fig. 4c, d, Supplementary Fig. 16a). These pulldowns show that MMACHC weakly interacts with MTR^{FL} (lane 7) whereas MMADHC appears to strongly interact (lane 8). To further confirm which halves of MTR are involved we carried out similar affinity-based pulldowns using MTR$^{N\text{-}Half}$ and MTR$^{C\text{-}Half}$ constructs (Fig. 4c, e). These pulldowns confirmed the weak, to potentially absent, interaction of MMACHC against the MTR$^{N\text{-}Half}$ and MTR$^{C\text{-}Half}$ constructs (Fig. 4e, Supplementary Fig. 16a), in which no positive pulldowns were observed (lanes 9, 11). Similar to previous published analyses on a C-terminal construct of MTR[17], we observed that MMADHC$^{\Delta N}$ interacts with MTR$^{C\text{-}Half}$ (lane 12) but not with MTR$^{N\text{-}Half}$ (lane 10). Overall, these collection of pulldowns are consistent with their corresponding AF3 predictions.

We next used size-exclusion gel filtration to determine the loading of HOCbl onto MTR^{FL} by MMADHC$^{\Delta N}$ (without a GST tag), through monitoring absorbance at 350 nm, indicative of the presence of Cbl. MTR^{FL} displays no absorbance at 350 nm, indicating that it is not bound to cobalamin (Fig. 4f upper left panel) agreeing with our native mass spectrometry measurements (Supplementary Fig. 1c). In the absence of MMADHC, low amounts of HOCbl binds MTR (Fig. 4f upper right panel) whereas MeCbl binds more readily (Fig. 4f lower left panel), agreeing with a previous analysis on a C-terminal construct of MTR[17]. When preincubated with MMADHC$^{\Delta N}$, HOCbl is loaded into MTR^{FL} through MMADHC$^{\Delta N}$, suggesting a direct interaction (Fig 4f lower right panel). Together our pulldown and Cbl loading experiments suggest that MTR not only interacts with MMADHC for Cbl loading but also appears to interact with MMADHC when Cbl is not present.

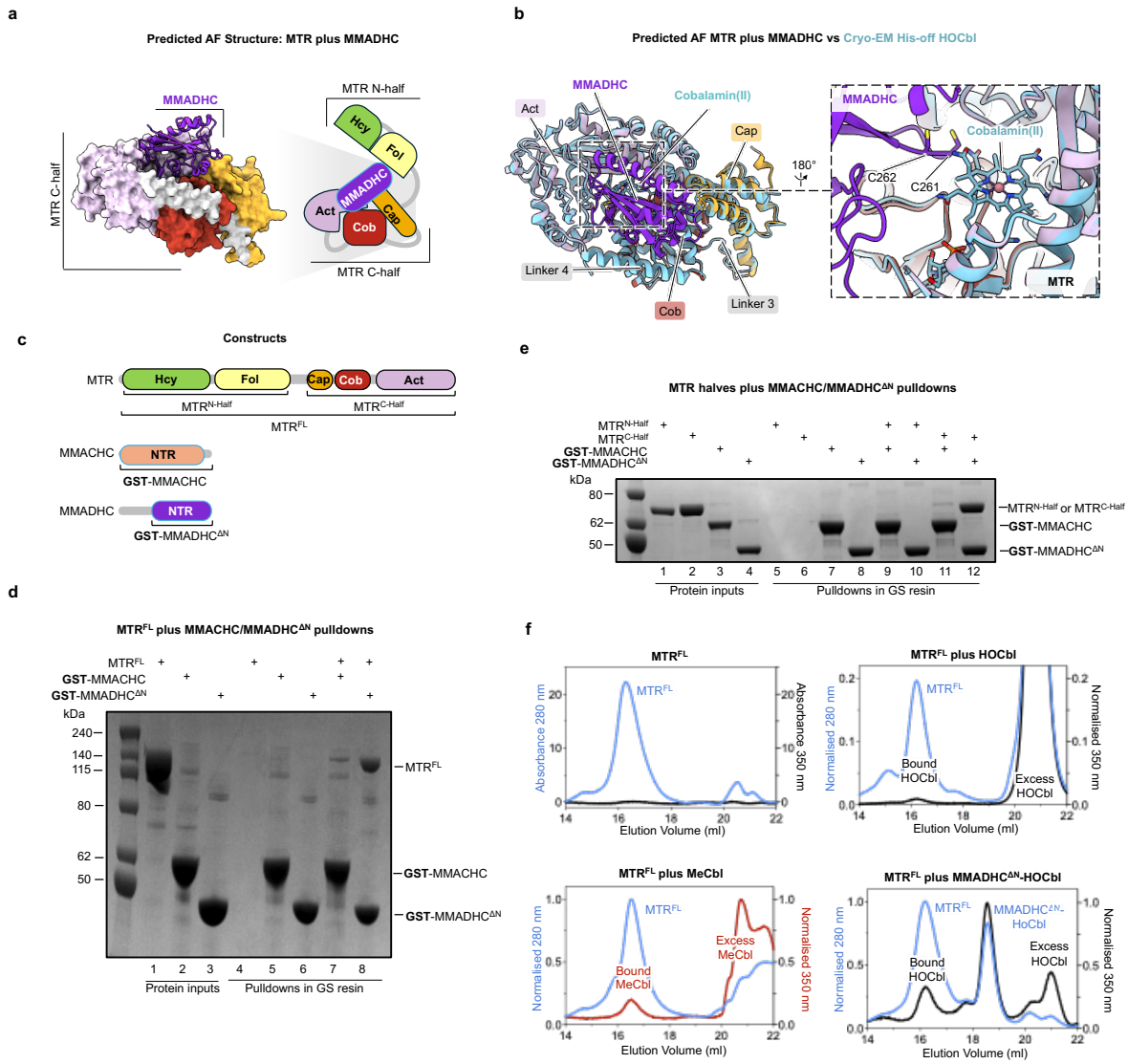

Fig. 4 | MMADHC forms a complex with MTR to load cobalamin. a, Representative predicted AF3 model of the MTR-MMADHC complex. The arrangement of the full-length complex is shown as a cartoon depicted with the domain colours as shown in Fig. 4a. The zoom-in cartoon shows only MTR$^{C\text{-}Half}$ with MMADHC; MMADHC is a ribbon model whereas MTR is shown as a surface model. **b,** Structural overlay of the predicted MTR$^{C\text{-}Half}$-MMADHC AF structure against our cryo-EM derived model of His-off MTR$^{C\text{-}Half}$. The zoom-in panel focuses on the MTR-MMADHC interface showing the relative location of the functionally important MMADHC residues C261 and C262. **c**, Constructs and domain arrangements of MTR, MMACHC, and MMADHC used in cobalamin transfer and pulldown assays. Affinity tagged constructs are indicated. **d,** GS resin affinity pulldown of MTR^{FL} against GST-MMACHC and GST-MMADHC$^{\Delta N}$. Lanes 1–3 represent the protein inputs used for the assay. Lanes 4–6 represent the elution fractions of each individual protein incubated with the resin to verify their ability to bind the resin. Lanes 7 and 8 represent the pulldown of MTR^{FL} with GST-MMACHC and the pulldown of MTR^{FL} with GST-MMADHC, respectively. **e,** GS resin affinity pulldown of MTR$^{N\text{-}Half}$ and MTR$^{C\text{-}Half}$ against the GST-MMACHC and GST-MMADHC$^{\Delta N}$. Lanes 1–4 represent the protein inputs used for the assay. Lanes 5–8 represent the elution fractions of each individual protein incubated with the resin to verify their ability to bind the resin. Lanes 9 and 10 represent the pulldown of MTR$^{N\text{-}Half}$ with GST-MMACHC and GST-MMADHC, respectively. Lanes 11 and 12 represent the pulldown of MTR$^{C\text{-}Half}$ with GST-

MMACHC and GST-MMADHC, respectively. **f,** Size-exclusion chromatography of cobalamin loading assay showing MTR^{FL}, MTR^{FL} plus HOCbl, MTR^{FL} plus MeCbl, and MTR^{FL} plus HOCbl-loaded $MMADHC^{\Delta N}$ monitored at 280 nm (blue) and 350 nm (black for HOCbl or red for MeCbl).

MTRR interacts with MTR through multiple domains

For the reactivation cycle, MTR requires the diflavin oxidoreductase MTRR to reduce the bound cob(II)alamin for methylation by SAM[19]. Beyond reports that the FMN domain of MTRR can interact with the Act domain of MTR[38], little is known on how MTRR interacts with MTR to transfer electrons from NADPH. To gain structural insights into their interactions we turned to AF3 to predict possible models of the MTR-MTRR complex.

AF3 modelling of the complex between MTR^{FL} and $MTRR^{FL}$ produced predicted models with moderate ipTM scores[36], in which the MTR N-half location varies between the individual predictions and the MTR C-half adopts a reactivation conformation (Fig. 5a, Supplementary Fig 17). Consistent across the five predicted structures is the relative location of MTRR where the MTRR FMN-binding domain is modelled to sit atop the MTR Cob domain and appears to interact with the Act domain (Fig. 5a). This agrees with previous biophysical studies demonstrating a physical interaction between the MTRR FMN domain and MTR Act domain[38]. To our surprise, the models reveal that in addition to the FMN domain, the other regions of MTRR (i.e. Conn domain, FAD domain, and NADPH domain; referred thereafter as MTRR ΔFMN) can also interact with MTR which was consistent across each prediction. This interaction occurs through two interfaces of MTRR ΔFMN, one involving the Conn domain that interacts with Linker 4 of MTR, and the other involving the NADPH domain that interacts with the MTR Cob domain. (Fig. 5a, 6a, Supplementary Fig. 17). This previously unidentified interaction was also consistently replicated in the AF3 modelling of complexes between the MTR C-half and the MTRR ΔFMN (Supplementary Fig. 18a). On the contrary, no consistent interactions with MTRR were predicted when the human MTR C-half sequence is replaced with bacterial MetH C-half sequences, suggesting that the interaction between the MTR C-half and MTRR ΔFMN is unique to eukaryotes (Supplementary Fig. 18b-d). Together, these predictions suggest that human MTRR interacts with human MTR, involving not only the FMN domain of MTRR, but also its C-terminal Conn, FAD, and NADPH domains.

To confirm these interactions *in vitro*, we used a combination of recombinant co-expression and reconstitution pulldown experiments. Firstly, co-expressing MTR^{FL} with $MTRR^{FL}$ in insect cells and purifying using the FLAG tag on MTR confirmed the presence of a complex without Cbl (Supplementary Fig. 19a). Additionally, in blue native PAGE experiments MTR^{FL} co-expressed with $MTRR^{FL}$ ran at a larger molecular weight than purified MTR^{FL} alone showing complex formation (Supplementary Fig. 19b). We then employed talon resin-based affinity pulldowns using purified $MTRR^{FL}$ as bait against the purified MTR^{FL}, $MTR^{N\text{-}Half}$, and $MTR^{C\text{-}Half}$ (Fig. 5b, Supplementary Fig. 19c), where $MTRR^{FL}$ showed an interaction with MTR^{FL} (Fig. 5c lane 9) and $MTR^{C\text{-}Half}$ (lane 11), but not $MTR^{N\text{-}Half}$ (lane 10). Importantly, these pulldown experiments confirm that the interaction between MTR and MTRR occurs through $MTR^{C\text{-}Half}$, even in the absence of Cbl or other ligands. Analytical size exclusion assays further confirmed that both full-length MTR and MTRR can form a complex (Fig. 5d left) specifically mediated by the C-half of MTR (right), but not its N-half (middle).

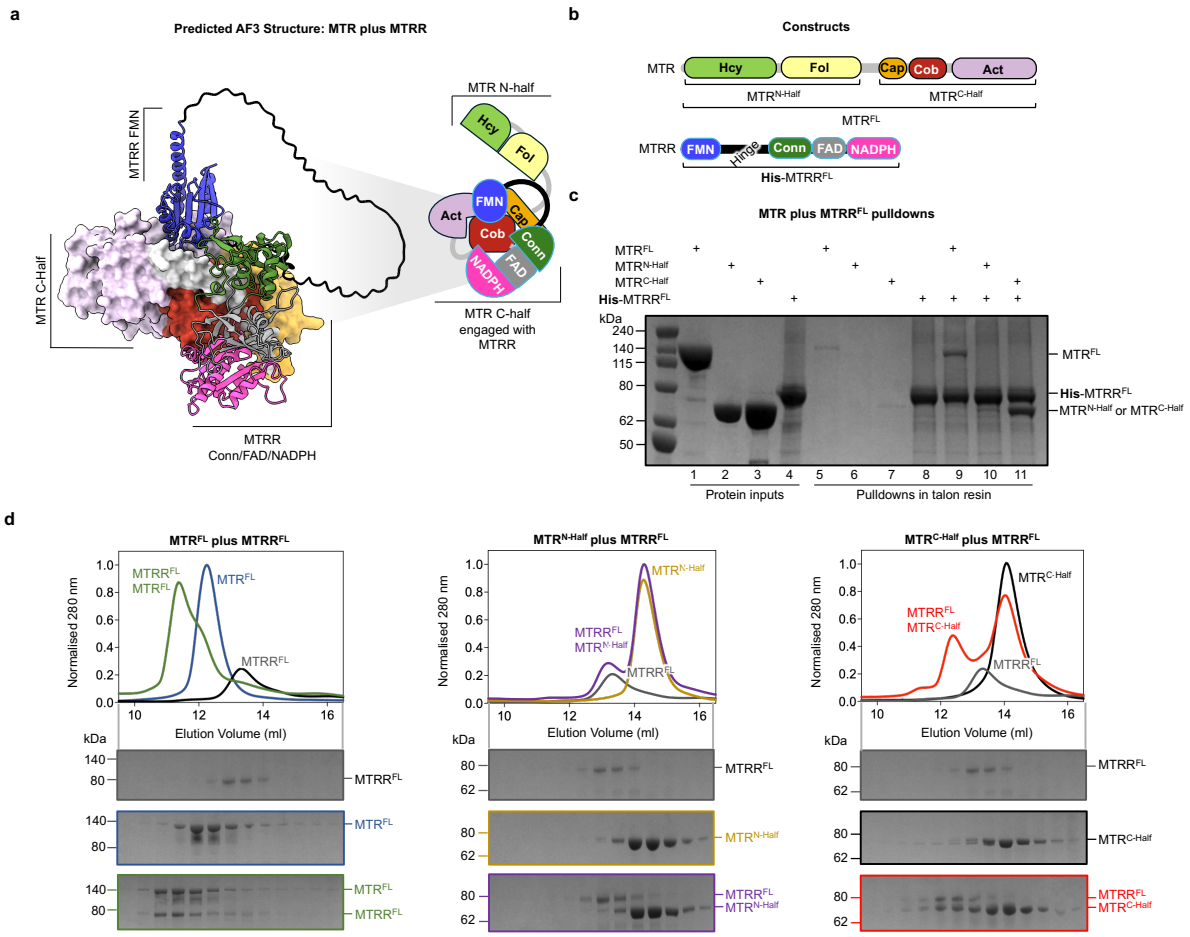

Fig. 5 | MTRR forms a stable complex with MTR. a, Constructs and domain arrangements of MTR and MTRR used in pull-down and gel filtration assays. Affinity tagged constructs are indicated. **b**, Representative predicted AF3 structure of the MTR-MTRR complex. The arrangement of the complex is shown as a cartoon depicted with the domain colours as shown in Fig. 5a. **c,** Talon resin affinity pulldown of the constructs shown in Fig. 5b. Lanes 1–4 represent the protein inputs used for the assay. Lanes 5–8 represent the elution fractions of each individual protein incubated with the resin to verify their ability to bind the resin. Lanes 9–11 represent the pulldown of the different protein combinations (His-MTRR^{FL} with MTR^{FL}, MTR$^{N\text{-}Half}$, or MTR$^{C\text{-}Half}$, respectively). **d,** Analytical size-exclusion chromatography of MTRR^{FL} in complex with MTR^{FL} (left), MTR$^{N\text{-}half}$ (middle), or MTR$^{C\text{-}half}$ (right). Top panels show the normalised spectrum at 280 nm and bottom panels show the corresponding SDS-PAGE of the eluted fractions.

To confirm the putative interaction between MTRR$^{\Delta FMN}$ and MTR, we expressed and purified a GST tagged construct of MTRR$^{\Delta FMN}$ (Fig. 6b, Supplementary Fig. 19d) for interaction studies. In GST pulldown experiments this construct showed an interaction with both MTR^{FL} (Fig. 6c lane 9) and MTR$^{C\text{-}Half}$ (lane 11), but not MTR$^{N\text{-}Half}$ (lane 10). Furthermore, analytical size exclusion using MTRR$^{\Delta FMN}$ without the GST tag confirmed the interactions of this region of MTRR with MTR^{FL} (Fig. 6d left) and MTR$^{C\text{-}Half}$ (right), but not with MTR$^{N\text{-}Half}$ (middle). Overall, our co-expression, pulldown, and gel filtration experiments are consistent with the AF3 predictions of the complex between MTR and MTRR.

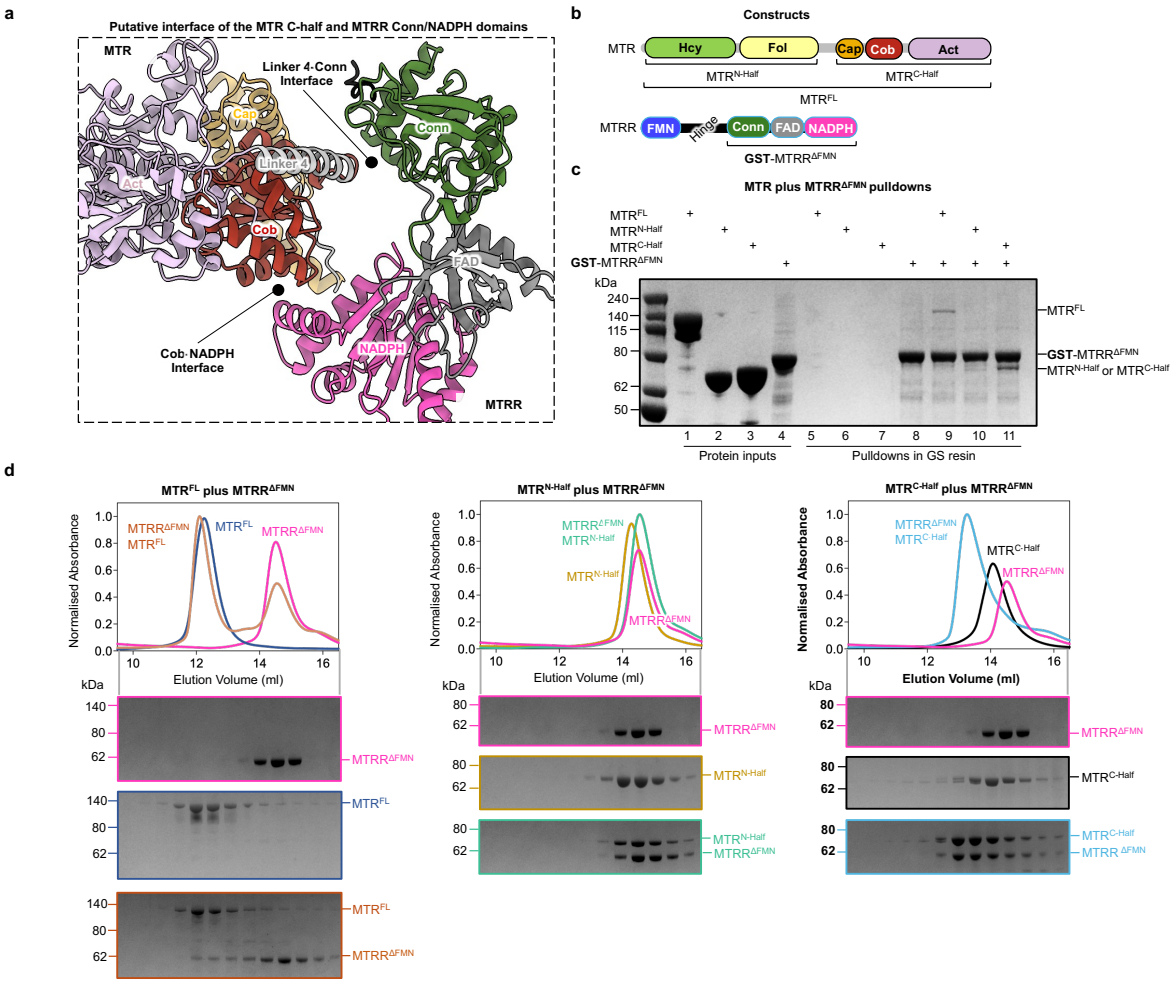

Fig. 6 | MTRR without the FMN domain can interact with MTR. a, Constructs and domain arrangements of MTR and MTRR used in pull-down and gel filtration assays. Affinity tagged constructs are indicated. **b**, Representative predicted AF3 structure of the MTR$^{C\text{-}half}$-MTRR$^{\Delta FMN}$ complex. The arrangement of the complex is shown as a cartoon depicted with the domain colours as shown in Fig. 6a. **c,** GS resin affinity pulldown of the constructs shown in Fig. 6b. Lanes 1–4 represent the protein inputs used for the assay. Lanes 5–8 represent the elution fractions of each individual protein incubated with the resin to verify their ability to bind the resin. Lanes 9–11 represent the pulldown of the different protein combinations (GST-MTRR$^{\Delta FMN}$ with MTR^{FL}, MTR$^{N\text{-}Half}$, or MTR$^{C\text{-}Half}$, respectively). **d,** Analytical size-exclusion chromatography of MTRR$^{\Delta FMN}$ in complex with MTR^{FL} (left), MTR$^{N\text{-}half}$ (middle), or MTR$^{C\text{-}half}$. Top panels show the normalised spectrum at 280 nm and bottom panels the corresponding SDS-PAGE analyses of the fractions indicated.

Discussion

Utilising vitamin B12 as a cofactor, MTR coordinates folate and methionine metabolism by performing three methylation reactions through its catalytic and reactivation cycles. Early x-ray crystallography and biochemical studies[9-11,39,40] on the bacterial homologue MetH demonstrated that the enzyme has structural modularity in order to carry out these reactions. Similarly, our cryo-EM data reveals human MTR to be modular comprising either of two or three independent modules linked by flexible linkers, representing inactive and active states respectively. Studies on MetH have suggested that when the enzyme is active, large conformational changes occur as the Cob domain shuttles between the Fol and Hcy domains to transfer a methyl group from MeTHF to Hcy using MeCbl during catalysis[9]. Every ~2000

508 reactions the bound cob(I)alamin intermediate can become oxidised to inactive
509 cob(II)alamin[32]. Reactivation requires another large conformational change that repositions
510 the Act domain to interact with the Cob domain to allow methylation of the inactive Cbl by
511 SAM[7]. These conformational changes are highly likely to be regulated and to be conserved in
512 human MTR. Although Cbl oxidation state and substrates have been suggested to be
513 important[40], little is known on how these conformational changes are triggered. Recent MetH
514 structures together with our findings are beginning to suggest a model for how these domain
515 movements are regulated (Figure 7).
516 Though of different conformational states, our structures are consistent with recent
517 reports of a tetra-domain structure of *T. filiformis* MetH[27], along with a full-length structure[24]
518 and multiple crystal structures of different constructs of *T. thermophilus* MetH bound to various
519 ligands[33] (Supplementary Fig. 20). Collectively these recent studies on thermophilic MetH
520 have revealed long sought structures of the full-length enzyme and snapshots of the Cob
521 domain engaged with either the Hcy or Fol domains giving insights into catalysis[33]. Surprisingly
522 a new conformation was initially reported by cryo-EM termed the "resting state" - a
523 hydroxycob(II)alamin bound, substrate free conformation where the Act domain is
524 disengaged, the Cap-on Cob module intimately interacts with the N-half, and a folate sensing
525 loop is positioned into the folate binding pocket (PDB 8G3H)[27]. This state was replicated by
526 crystallisation with a MetH construct without the Act domain and bound to
527 propylcob(III)alamain (PDB 9CBP). Two additional crystal structures of a MetH Fol-Cap-Cob
528 construct bound to MeCbl in a Cap-on conformation were also determined (PDB 9CBO)[33].
529 These states were subsequently termed "gating states" as they are assumed to be the "Hcy-
530 gate" (PDB 9CBP), "Fol-gate" (PDB 9CBO), and "Act-gate" (PDB 9CBO) before the
531 conformational change to the Hcy-on, Fol-on, and Act-on states respectively[33]. However, both
532 "resting state/Hcy-gate" structures are of inactive Cbl forms without any bound substrates.
533 This means they are more likely representative of the enzyme inactivated by oxidation and of
534 the cob(I)alamin state before the binding of MeTHF. Therefore this conformation is likely the
535 shared conformation between the catalytic and reactivation cycles[27] as the "Act-gate" (i.e.
536 before reactivation) and "Fol-gate" (i.e. before catalysis) depending on the oxidation of Cbl.
537 Favouring this interpretation is that *E. coli* MetH shows ordered ping-pong kinetics
538 where MeTHF is the first substrate to bind and THF is the last product to leave[41] meaning that
539 the resting state/Hcy-gate structures are not substrate bound intermediates during catalysis.
540 Additionally, it is likely the probability of oxidation of the bound cob(I)alamin is increased when
541 MeTHF is limited, and a recent study showed that the rate of reactivation for human MTR is
542 increased in the presence of both the substrate MeTHF and the product THF[42]. This increased
543 reactivation likely occurs due to substrate binding to the Fol domain and displacing the folate
544 sensing loop[27] allowing the formation of a Cap-off Act-on state productive for reactivation. A
545 similar conformational change due to MeTHF binding to the cob(I)alamin state would occur
546 resulting in a Fol-on conformation. In the reported "Fol-gate" and "Act-gate" MeCbl bound
547 crystal structures, the folate sensing loop is not displaced into the folate binding pocket
548 suggesting that folate binding has little to no influence in any structural transitions in these
549 states[33]. The two structures also have different relative orientations of the Fol domain to the
550 Cap-on Cob domain module suggestive of flexibility (Supplementary Fig. 20). These structures
551 are consistent with our MeCbl cryo-EM data of human MTR where the folate sensing loop has
552 not moved into the Fol binding pocket, and the activation domain is disengaged from the highly
553 flexible Cap-on Cob domain module. This conformation along with the crystal structures are
554 more aptly termed the "Hcy-gate" as the enzyme is bound to MeCbl, a form productive for
555 methyl transfer to the substrate Hcy. The MeCbl bound enzyme without bound folate forms
556 this more flexible state instead of the more compact "resting-state" likely due to the distance
557 that the Cob domain has to travel between the Fol and Hcy domains (~50 Å) during the
558 catalytic cycle.
559 Although both MetH and MTR share similar reactivation conformations, prior to
560 receiving Cbl, MetH does not require a highly specialised chaperone to load the cofactor[43].
561 MMADHC has a central role in Cbl trafficking in eukaryotes and is known to direct the co-
562 factor to either methylmalonyl-CoA mutase (MMUT) in the mitochondria or MTR in the

563 cytosol[14]. AlphaFold predictions suggest that MMADHC engages the exposed Cbl-binding
564 pocket via all three domains in the C-half of MTR when in a reactivation conformation. This
565 interaction model aligns with experimental data on Cbl loading, suggesting a structural
566 rationale for how MMADHC and MTR form a complex.
567 Cbl is loaded as a cob(I)alamin onto MTR, but most of it is readily oxidised into
568 cob(II)alamin[17] which cannot support catalysis. The reductive methylation of cob(II)alamin,
569 required for the reactivation, is assisted by electron transfer from the essential flavoprotein
570 MTRR[20]. MTRR is an unusual member of the diflavin reductase family where it has a much
571 longer hinge region than expected between the N-terminal FMN domain and the rest of the
572 enzyme[44]. Previous studies revealed that the FMN-binding domain of MTRR engages with
573 MTR to reduce the cobalamin, which is subsequently methylated to MeCbl[38]. Our predictive
574 modelling and biophysical analyses of the MTR-MTRR complex revealed previous unknown
575 interacting interfaces between these proteins and explains its long hinge region. AF3 structure
576 predictions suggested that MTRR can also interact with MTR through its NADPH-binding and
577 connecting domains when the FMN domain is engaged. This unexpected interaction was
578 confirmed by our biophysical assays using truncated constructs. These additional interfaces
579 could indicate a mechanism of MTR to optimize the efficiency of the reductive methylation by
580 forming a stable complex with MTRR even prior to entering the reactivation cycle. This
581 interaction is not predicted between MTRR and MetH, which relies on a different reactivation
582 system supported by flavodoxin[21]. The fact that MTR cannot be reactivated by flavodoxin, and
583 conversely MetH cannot be reactivated by MTRR, suggests that this new identified interaction
584 may be essential for Cbl reduction[25]. This lack of cross-reactivity could be due to the lower
585 conservation in the region of MTR responsible for this extended interaction with MTRR
586 (Supplementary Fig. 21 α-helix 35).
587 Figure 7 integrates our cryo-EM snapshots, AF3 predictions, biophysical data, and
588 interpretation of previous studies along with other structures into a proposed stepwise
589 mechanism, for Cbl loading, reactivation, and catalysis: During cobalamin loading (i), apo MTR
590 is poised in the Cap-off reactivation conformation, ready to interact with MMADHC for
591 receiving Cbl. MMADHC loads cob(I)alamin which without SAM can be readily oxidised to
592 cob(II)alamin. Therefore, during the reactivation cycle (ii) MTR still in the reactivation
593 conformation is ready to interact with MTRR, for the reductive methylation of the bound Cbl
594 using SAM. This interaction is secured by two interacting sites and allows an efficient electron
595 transfer from the FMN-binding domain of MTRR to the Cbl. Following Cbl methylation, MTR
596 undergoes a large conformational change as the bound Cbl goes from His-off to His-on,
597 triggering MTRR unbinding. This results in the flexible MeCbl bound state (Hcy-gate), where
598 the Act and Cob domains disengage, and the Cap domain takes place atop the Cbl, protecting
599 it from oxidation before beginning catalysis. This places MTR within the catalytic cycle (iii)
600 ready to engage with the Hcy domain to carry out a methyl transfer reaction to form
601 methionine. After this the substrates leave MTR and result in a “Fol-gate” Cap-on conformation
602 to protect the cob(I)alamin intermediate. If oxidation has occurred to produce cob(II)alamin
603 MTR forms the same conformation with different responses to the binding of the substrate
604 MeTHF. In cob(I)alamin bound MTR MeTHF binding to the Fol domain disrupts its interaction
605 with the Cap and Cob domains to promote a “Fol-on” conformation to produce MeCbl and
606 continue another catalytic cycle. In cob(II)alamin bound MTR MeTHF binding to the Fol
607 domain also disrupts its interaction with the Cap and Cob domains but promotes the Act-on
608 reactivation conformation which allows MTR to enter the reactivation cycle.

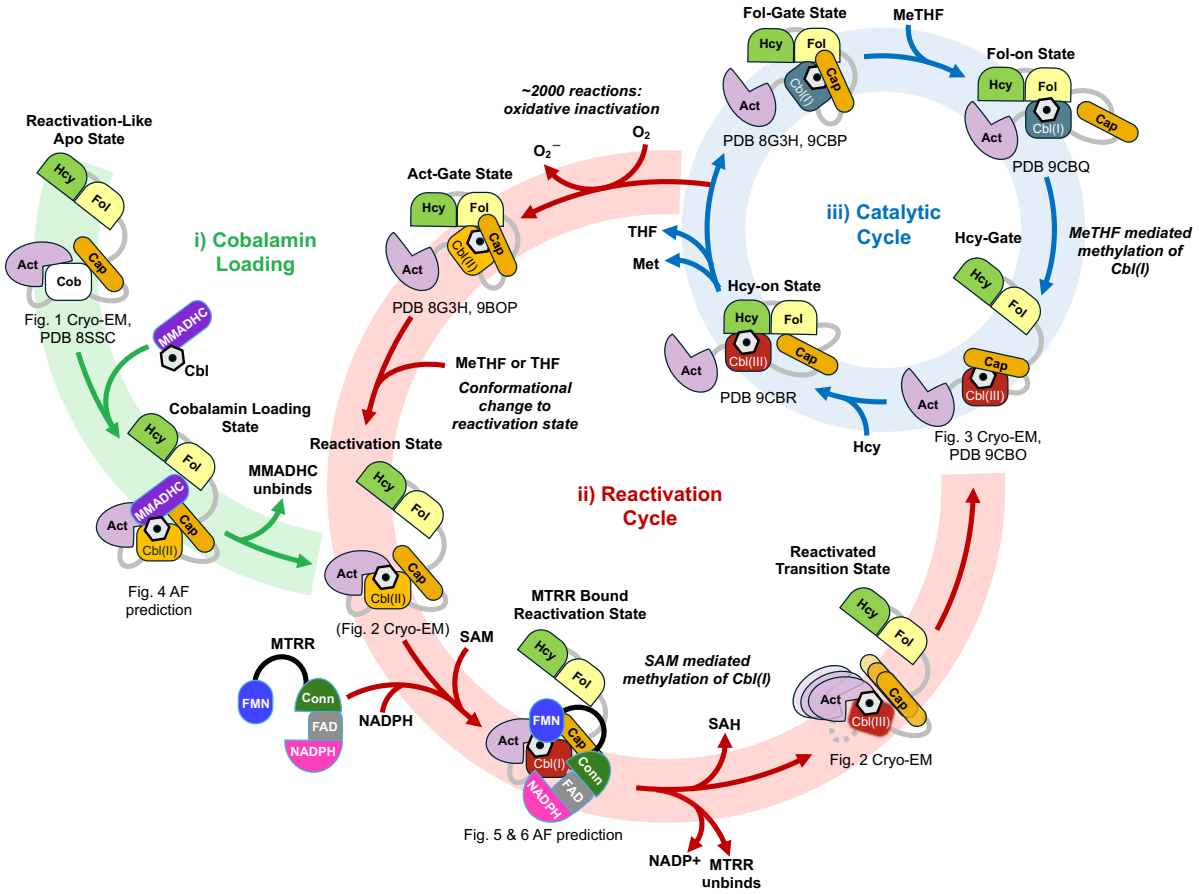

Fig. 7 | Proposed mechanism of cobalamin loading, reactivation, and catalysis of MTR. Model showing various cartoons of proposed conformations and complexes for human MTR with MMADHC and MTRR for three major aspects of its function: i) cobalamin loading, ii) reactivation cycle, and iii) catalytic cycle. Please read the main text for more details for each aspect. Different Cbl oxidation states are stated and represented as light orange for cob(II)alamin, red for cob(III)alamin, and dark cyan for cob(I)alamin. Domains are coloured as previously depicted in previous figures. This proposed mechanism is not comprehensive. Therefore, other conformations and complexes may also occur.

Though our proposed mechanism attempts to show how MTR goes from a Cbl free apo state to a MeCbl bound active state there are a number of caveats and unanswered questions. While our cryo-EM structures show for the first time Cbl binding of human MTR and its intrinsic flexibility these structures are determined from using free Cbl in solution and thus may not be fully representative of when Cbl is loaded by MMADHC and reactivated by MTRR. Additionally, we have only carried out interaction studies between MTR and its proposed interacting partners without any ligands, which may alter how these proteins interact. MMACHC may stably interact with MTR when MMADHC is present as a ternary complex[14,15] with possible consequences for cofactor loading. The findings that both MMADHC and MTRR can bind to MTR without any bound Cbl also suggests that these proteins may have further roles beyond loading and reactivation. Supporting this hypothesis is a previous report which suggested that MTRR acts as a chaperone of apo MTR as it increases MTR's stability[25]. A recent study also proposed a chaperone role of MMADHC for MTR[42]. This leads to the possibility of ternary complexes where an apo complex of MTR and MTRR may interact with apo or Cbl bound MMADHC. This is also underlined by reports of a quaternary complex of all of four proteins[12]. Another report suggested a direct interaction of MMACHC with MTR[35]. However, this does not appear to be supported by our AF3 predictions and pulldown assays where MMACHC shows little to no interaction.

638 Overall, our findings expand current knowledge on human MTR and contextualize
639 previous reported findings on both it and its bacterial homologues. Importantly we reveal
640 insights into eukaryotic unique aspects in terms of the complexes that MTR forms to support
641 its function. Given that pathogenic mutations in MTR, MTRR, MMACHC, and MMADHC are
642 linked to Cbl deficiency it is likely that some mutants effect residues at protein-protein
643 interfaces of these MTR complexes. Indeed, variants of MMADHC have been suggested to
644 weaken its interaction with MTR hindering Cbl loading[17]. Consequently, future experimental
645 structure determination of the MTR complexes with MMADHC and MTRR will be essential in
646 understanding how pathogenic mutants alter their complex formation. Such molecular insights
647 could inform the development of targeted therapies towards the treatment of these rare
648 metabolic disorders.
649

650 **Methods**

651 **Cloning, expression, and purification of MTR constructs**

652 Full-length MTR (MTR^{FL}) for cryo-EM, activity, and thermal stability assays was cloned into
653 pFB-CT10HF-LIC encoding for a C-terminal TEV cleavable His-tag and FLAG-tag for insect
654 cell expression. MTR^{FL} was expressed in Sf9 cells infected with P3 baculovirus and grown in
655 Sf-900 III SFM (Life Technologies) for 72 hrs. Cell pellets were harvested and homogenized
656 in lysis buffer (50 mM HEPES pH 7.5, 500 mM NaCl, 5% glycerol, 0.5 mM Tris(2-
657 carboxyethyl)phosphine hydrochloride (TCEP) and 20 mM imidazole) using sonication, and
658 insoluble material was removed by centrifugation. MTR was then purified by affinity (Ni-
659 sepharose; Cytiva) and size-exclusion (Superdex 200; Cytiva) chromatography to separate
660 monomeric MTR from aggregates. Purified MTR^{FL} was then concentrated to 3–10 mg/ml,
661 aliquoted, and stored in storage buffer (50 mM HEPES pH 7.5, 500 mM NaCl, 5% glycerol,
662 0.5 mM TCEP) at −80 °C.

663 Full-length MTR (MTR^{FL}) for pull-down and gel filtration assays, was cloned into pNIC-
664 CT10HSII encoding for a C-terminal TEV cleavable His-tag and tandem StrepII-tag for
665 bacterial expression. MTR^{FL} was expressed in ArcticExpress DE3 cells. Cells were cultured in
666 Terrific Broth (Formedium) at 30 °C in Terrific Broth and expression was carried out for 60 hrs
667 at 10 °C induced with 0.1 mM isopropyl-β-D-thiogalactopyranoside (IPTG). Cell pellets were
668 harvested and homogenized in lysis buffer (50 mM sodium phosphate pH 7.5, 500 mM NaCl,
669 5% glycerol, 0.5 mM TCEP, 1.0 % triton X-100, and 20 mM imidazole) using sonication, and
670 insoluble material was removed by centrifugation. MTR^{FL} was then purified from the
671 supernatant by tandem affinity using Ni-sepharose followed by Streptactin XT resin (Cytiva).
672 MTR^{FL} was then treated with His-tagged TEV protease overnight at 4 °C and passed over Ni-
673 sepharose resin to remove the TEV protease and any uncleaved protein. A final size-exclusion
674 (Superdex 200; Cytiva) chromatography step was used to separate monomeric MTR^{FL} from
675 degradation products. Purified MTR^{FL} was then concentrated to 3–10 mg/ml, aliquoted, and
676 stored in storage buffer (50 mM HEPES pH 7.5, 500 mM NaCl, 5% glycerol, 0.5 mM TCEP) at
677 −80 °C.

678 The N-terminal construct of MTR, residues 16-657 ($MTR^{N\text{-}Half}$), was cloned into pNIC-
679 Bsa4 encoding for a N-terminal TEV cleavable His-tag. The C-terminal construct of MTR,
680 residues 661-1265, ($MTR^{C\text{-}Half}$) was cloned and into pNIC-CH as a TEV cleavable His-GST N-
681 terminally tagged for bacterial expression (Twist Bioscience). A stop codon was added at the
682 end of the $MTR^{C\text{-}Half}$ coding sequence before the vector encoded His-tag. Both constructs were
683 expressed in Rosetta DE3 cells. Cells were cultured in Terrific Broth (Formedium) at 37 °C
684 and expression was induced overnight at 18 °C with 0.2 mM IPTG. Pellets were harvested,
685 homogenized in lysis buffer (50 mM HEPES pH 7.5, 500 mM NaCl, 5% glycerol, 0.5 mM TCEP
686 and 20 mM imidazole) by sonication, and insoluble material was removed by centrifugation.
687 The supernatant was subjected to affinity (Ni-sepharose; Cytiva) and the eluted protein
688 applied to size-exclusion (Superdex 200; Cytiva) chromatography. Each construct was then
689 treated with His-tagged TEV protease overnight at 4 °C and passed over Ni-sepharose resin
690 to remove the TEV protease and uncleaved protein. In some incidences, an additional size-
691 exclusion step was carried out to remove residual TEV protease. Purified $MTR^{N\text{-}Half}$ and $MTR^{C\text{-}}$

692 ^{Half} proteins were concentrated to 10–20 mg/ml and stored in storage buffer (50 mM HEPES
693 pH 7.5, 500 mM NaCl, 5% glycerol, 0.5 mM TCEP) at −80 °C.
694
695 **Cloning, expression, and purification of MTRR constructs**
696 Full-length codon optimised MTRR ($MTRR^{FL}$) was cloned into pFastBac (Genscript) encoding
697 for a TEV cleavable N-terminal His-tag and was expressed in Sf9 cells grown in Sf-900 III
698 SFM (Life Technologies) for 72 hrs. Cell pellets were harvested and resuspended in lysis
699 buffer (50 mM sodium phosphate pH 7.5, 500 mM NaCl, 5% glycerol, 0.5 mM TCEP, 1.0%
700 triton x-100, 100 µM flavin mononucleotide). The resuspended pellet was incubated at room
701 temperature for 30 minutes with spinning, followed by sonication, and then subsequent
702 centrifugation to remove insoluble material. $MTRR^{FL}$ was then purified from the soluble fraction
703 by affinity (Ni-sepharose; Cytiva). Purified $MTRR^{FL}$ was then diluted in low salt buffer (50 mM
704 HEPES pH 7.5, 50 mM NaCl, 5% glycerol, 0.5 mM TCEP) and applied to a HiTrap Q column
705 (Cytiva). A gradient from 50 mM to 1M NaCl was used to elute $MTRR^{FL}$. Appropriate fractions
706 were pooled, concentrated, and buffer exchanged into storage buffer (50 mM HEPES pH 7.5,
707 500 mM NaCl, 5% glycerol, 0.5 mM TCEP.)
708 The MTRR construct without the FMN domain, residues 217-698, ($MTRR^{\Delta FMN}$) was
709 cloned from a codon optimised sequence (Twist Bioscience) into pGTVL2 to produce a TEV
710 cleavable His-GST N-terminally tagged protein for bacterial expression. $MTRR^{\Delta FMN}$ was
711 expressed in Rosetta DE3 cells. Cells were cultured in Terrific Broth (Formedium) at 37 °C
712 and expression was induced overnight at 18 °C with 0.2 mM IPTG. Pellets were harvested,
713 homogenized in lysis buffer (50 mM sodium phosphate pH 7.5, 500 mM NaCl, 5% glycerol,
714 0.5 mM TCEP, 1.0% triton X-100, and 20 mM imidazole) by sonication, and insoluble material
715 was removed by centrifugation. To produce tagged protein for pull-down assays the
716 supernatant was subjected to affinity (Ni-sepharose; Cytiva) and the eluted protein was further
717 purified by anion exchange using a HiTrap Q column (Cytiva). Clean fractions containing the
718 GST tagged construct were pooled and further treated to size-exclusion (Superdex 200;
719 Cytiva) chromatography. To produce cleaved $MTRR^{\Delta FMN}$ protein for analytical gel filtration
720 assays the supernatant was subjected to affinity (Ni-sepharose; Cytiva), and the eluted protein
721 incubated with His-tagged TEV protease overnight at 4 °C. The cleaved protein was then
722 subjected to size-exclusion (Superdex 200; Cytiva) chromatography. Peak fractions of cleaved
723 $MTRR^{\Delta FMN}$ were pooled and passed over Ni-sepharose resin to remove any remaining TEV
724 protease. Both the tagged and cleaved $MTRR^{\Delta FMN}$ proteins were concentrated to 5-10 mg/ml
725 and stored in storage buffer (50 mM HEPES pH 7.5, 500 mM NaCl, 5% glycerol, 0.5 mM
726 TCEP) at −80 °C.
727
728 **Co-expression, and purification of the MTR-MTRR complex**
729 Using the biGBac cloning system the genes for full-length MTR and full-length MTRR were
730 cloned into pBIG1a. The MTR^{FL} gene encoded for a C-terminal TEV cleavable His and FLAG
731 whereas the MTRRFL gene encoded a N-terminal His-tag. The MTR^{FL}-$MTRR^{FL}$ complex was
732 expressed in Sf9 cells grown in Sf-900 III SFM (Life Technologies) for 72 hrs. Cell pellets were
733 harvested and homogenized in lysis buffer (50 mM HEPES pH 7.5, 500 mM NaCl, 5% glycerol,
734 0.5 mM TCEP) using sonication, and insoluble material was removed by centrifugation. The
735 complex was then purified by affinity (Ni-sepharose; GE Healthcare) and size-exclusion
736 (Superdex 200; GE Healthcare) chromatography. Fractions corresponding to the complex
737 were pooled, concentrated to 5–10 mg/ml and stored in storage buffer (50 mM HEPES pH 7.5,
738 500 mM NaCl, 5% glycerol, 0.5 mM TCEP) at −80 °C.
739
740 **Cloning, expression, and purification of MMACHC and $MMADHC^{\Delta N}$**
741 The cloning, expression, and purification of MMACHC and $MMADHC^{\Delta N}$ (residues 124-296)
742 has been described in detail elsewhere[13,14]. In brief His-GST tagged MMACHC and
743 $MMADHC^{\Delta N}$ were expressed in Rosetta DE3 cells. Cells were cultured in Terrific Broth
744 (Formedium) at 37 °C and expression was induced overnight at 18 °C with 0.1 mM IPTG.
745 Pellets were harvested, homogenized in lysis buffer (50 mM HEPES pH 7.5, 500 mM NaCl,
746 5% glycerol, 0.5 mM TCEP and 20 mM imidazole) by sonication, and insoluble material was

removed by centrifugation. The supernatant was subjected affinity (Ni-sepharose; Cytiva) and the eluted protein applied to size-exclusion (Superdex 200; Cytiva) chromatography. To produce cleaved MMADHC$^{\Delta N}$ the His-GST tagged protein after size exclusion was treated with His-tagged TEV protease overnight at 4 °C and passed over Ni-sepharose resin to remove the TEV protease and uncleaved protein. Purified tagged MMACHC, tagged MMADHC$^{\Delta N}$, and cleaved MMADHC$^{\Delta N}$ proteins were concentrated to 10–20 mg/ml and stored in storage buffer (50 mM HEPES pH 7.5, 500 mM NaCl, 5% glycerol, 0.5 mM TCEP) at −80 °C.

Native mass spectrometry

By dialysis, purified MTR^{FL} was exchanged from into 50 mM ammonium acetate, pH 6.5. The sample was loaded into Quantitative Time-of-Flight (Q-TOF) 6530 mass spectrometer attached to a standard electrospray ionisation source (Agilent Technologies), with 77 a constant flow rate of 6 µl min^{-1}, using a 1.0-ml gas-tight positive displacement syringe (Hamilton) and PEEK capillary tubing with an inner diameter of 0.005 inches.

Enzyme activity assay

MTR activity assay was adapted from the previously described cuvette-based nonradioactive assay[26]. The current assay was miniaturised for a U-bottom 96-well plate. The following reagents were added to each well in the mentioned order: 24.4 µL of 100 mM phosphate buffered saline (PBS) pH 7.5, 2 µL of 500 mM dithiothreitol (DTT), 2 µL of 3.8 mM S-adenosylmethionine (SAM), 2 µL of 100 mM L-homocysteine (Hcy), 5 µL of 4 µM MTRF^{L}, and 4 µL of 500 µM HOCbl. The plate was then incubated for 5 minutes at 37 °C, allowing DTT and HOCbl to create a semi-anaerobic environment by reducing O_2 into H_2O_2. After this time, 2.4 µL of 6.6 mM 5-methyltetrahydrofolate (MeTHF) was added to initiate the catalytic cycle of MTR, thus producing tetrahydrofolate. After 10 minutes at 37 °C, the reaction was quenched by adding 10 µL of 5 M HCl in aqueous 60% formic acid and immediately heated at 80 °C for 10 minutes to convert the produced tetrahydrofolate to methenyltetrahydrofolate, which concentration can be determined using $\Delta\varepsilon 350 = 26{,}500\ M^{-1}\ cm^{-1}$. Absorbance was recorded on a OmegaSTAR (BMG Biotech), which were pathlength corrected. The data was analysed and plotted on GraphPad Prism 10.

Thermal shift assay

MTR proteins were diluted in thermal shift buffer (25 mM HEPES, pH 7.5, 200 mM NaCl) to 0.4 mg/ml with SYPRO-Orange (Invitrogen) diluted 1000X in a total volume of 20 µl. When appropriate, ligands were added at a final concentration of 1 mM, except for HOCbl, CNCbl, and MeCbl which were added at a final concentration of 50 µM. A QuantStudio 3 RT-PCR machine (Thermo Fisher Scientific) was used to monitor protein melting across 25 °C – 95 °C with a heating rate of 0.5 °C per min. Data were analysed in GraphPad Prism software, and the thermal melting temperatures (T_m) were determined using a nonlinear Boltzmann equation.

Negative stain electron microscopy

Purified recombinant monomeric MTR^{FL} from size exclusion chromatography was diluted to a final concentration of 40 nM in buffer (25 mM HEPES pH 7.5, 250 mM NaCl). 10 µl sample was added to copper grids with carbon coating (300 mesh, Quantifoil Micro Tools GmbH), plasma treated for 1 min using PELCO easiGlow™ (Ted Pella, Inc). After 30 seconds excess sample was dried off using filter paper (Whatman), and the grid was placed on a drop of filtered 1.5 % uranyl acetate (Sigma-Aldrich) for 30 seconds. Grids were dried again using filter paper before visualisation. Imaging was performed using a Hitachi HT7800 microscope operating at 120 kV and with a magnification of 60k, located at the Electron Microscopy Research Services (EMRS) facility at Newcastle University.

Grid preparation and cryo-electron microscopy

MTR^{FL} was diluted to 0.5 mg/ml into 25 mM HEPES, pH 7.5, 250 mM NaCl with either 1 mM MeTHF, 1 mM MeTHF, 1 mM SAM and 50 µM HOCbl, or 50 µM MeCbl. Grids were prepared

using a FEI Vitrobot Mark III (Thermo Fisher Scientific) at 4 °C and 100% humidity. 3 µl of sample was applied to a plasma treated R1.2/1.3 300 mesh UltrAuFoil (Quantifoil) grid, with a blot force of 0, a blot time of 3 seconds and a wait time of 10 seconds. All grids were initially screened by collecting a small ≈ 1,000 micrograph dataset on a 200 kV Glacios microscope equipped with a Falcon 4 direct electron detector (ThermoFisher Scientific) at York Structural Biology Laboratory. Data was collected at a magnification of 240k with a pixel size of 0.574 Å and a total dose of 50 $e^-/Å^2$. Glacios data was processed in cryoSPARC[45] and only grids that resulted in clear 2D classes were sent for larger data collections on a 300 keV Krios microscope.

All high-resolution data collection was carried out at Electron Bio-Imaging Centre (eBIC, Diamond Light Source, UK). For MTR^{FL} with MeTHF, and MTR^{FL} with MeTHF, SAM and HOCbl were collected on a 300 kV Titan Krios equipped with a K3 direct electron detector and energy filter (Gatan). K3 data was collected at a magnification of 165k equating to a pixel size of 0.508 Å (super resolution mode 0.254 Å) with an exposure time of 1.00 s, and a total dose of 65.20 $e^-/Å^2$. For MTR^{FL} with MeCbl data was collected on a 300 kV Titan Krios equipped with a Falcon 4i direct electron detector and selectris X energy filter (ThermoFisher Scientific). Falcon 4i data was collected at a magnification of 215k equating to a pixel size of 0.576 Å with an exposure time of 2.46 s and a total dose of 70 $e^-/Å^2$.

Data processing for each dataset followed the same following general process: All movies were imported into cryoSPARC[45] where they were subjected to patch motion correction and patch CTF estimation. Micrographs were into 2,000 micrograph subsets for particle picking, extraction, and 2D classification. All 2D classifications used the standard preset parameters expect that force over max poses/shifts was turned off, the number of online-EM iterations was increased from 20 to 40, the number of full EM iterations was increased from 1 to 3, and the batch size was increased to 400. Initially blob picking was used on each micrograph subset. Particles were extracted in a 400-pixel box Fourier cropped to 200 pixels and subjected to multiple rounds of 2D classification to remove bad picks and junk. Once good 2D classes were determined it was clear that two types of particles were present in each dataset. Separate 2D classes for these particle types were used for separate template-based picking which were then again extracted in a 400-pixel box Fourier cropped to 200 pixels and subjected to rounds of 2D classification. Finally for both particle types, these particles were used in combination with Topaz[46] to pick particles that were missed or poorly centred by blob and template picking. Again, these particles were extracted in a 400-pixel box Fourier cropped to 200 pixels and subjected to rounds of 2D classification. For each particle type particles from blob, template, and Topaz[46] based picking were separately pooled, duplicates removed and subjected to another round of 2D classification. Ab-initio with three to six classes followed by heterogenous refinement was used to determine the best particles that were then subjected to non-uniform refinement followed by local refinement. Reference based motion correction was then used followed by another round of ab-initio, heterogenous, non-uniform, and local refinement. In the case of the $MTR^{C\text{-}Half}$ maps 3D variability analysis[30] was carried out with 3 components filtered to 5.0 Å. For the $MTR^{C\text{-}Half}$ map from the MeTHF, SAM, and HOCbl dataset 3D variability was done in cluster mode followed by local refinement. One cluster equated to the His-off state whereas one cluster equated to the His-on state. As none of the maps reached Nyquist the extracted particle images were left Fourier cropped meaning that maps from the K3 datasets have a pixel size of 1.016 Å and the Falcon 4i maps have a pixel size of 1.152 Å. More details are shown in the supplementary information (Supplementary Fig. 3, 5, and 8). Local resolution, conical FSC area ratio (cFR), and sampling compensation factor (SCF) were determined within cryoSPARC[45] for each map (Supplementary Fig. 9).

Atomic model fitting, refinement, and validation

For all MTR structures described we used the predicted AlphaFold structure of MTR^{FL} (Q99707)[47] as an initial starting model. For each map the appropriate domains were manually fitted and docked using ChimeraX[48]. Isolde[49] global flexible fitting was then carried out followed by real space refinement as implemented in Phenix[50]. Ramachandran outliers were inspected

and manually corrected in Coot[51] followed by a final Phenix real space refinement. For the ligands methyltetrahydofolate and cobalamin, Phenix eLBOW[52] was used to produce their restraints. Each ligand was manually docked into their appropriate density using Coot and were subjected to rounds of manual refinement and Phenix real space refinement. All models were validated using Molprobity[53]. Model fit was assessed by model to map FSC determination in Phenix[50] and using the Q-score[54] implementation in ChimeraX[48] (Supplementary Fig. 10)

Structure prediction using AlphaFold3

The AlphaFold3 server[36] was used to predict the complex structures of MTR (Q99707-1), MTRR (Q9UBK8-2), MMACHC (Q9Y4U1), and MMADHC (Q9H3L0) using their amino acid sequences as input. The sequences of MTR from *Thermus thermophilus* (Q9RA53), *T. filiformis* (A0A0A2XCD7), and *Escherichia coli* (P13009) were also used for the complex prediction studies. In some incidences the sequences corresponding to the boundaries of $MTR^{N\text{-}Half}$, $MTR^{C\text{-}Half}$, and $MTRR^{\Delta FMN}$ were used. All five output models for each prediction were manually inspected in ChimeraX[48]. pLDDT[55] values from the server were used to analyse the confidence of modelling for individual proteins. Both pTM and ipTM scores calculated from the server were used to judge the confidence of each predicted complex structure[36,56,57].

Blue native-PAGE

Blue native-PAGE was carried out according to manufacturer's instructions (Life Technologies). Both MTR^{FL} and the MTR^{FL}-$MTRR^{FL}$ complex expressed and purified from insect cells were diluted to 1.0 mg/ml in 25 mM HEPES, pH 7.5, 250 mM NaCl.

Talon pull-down assay

The bait, $MTRR^{FL}$ with a N-terminal His-tag at 0.5 mg ml^{-1} was mixed with either prey proteins MTR^{FL}, $MTR^{N\text{-}Half}$ or $MTR^{C\text{-}Half}$ without His-tags at 0.5 mg ml^{-1} in a total volume of 100 µl diluted in binding buffer (25 mM HEPES, pH 7.5, 100 mM NaCl, 1 mM TCEP, 0.2% Tween-20). Protein mixes were incubated with rotation at room temperature for 30 min. Next, 80 µl of a 50% slurry of talon resin (Clontech) in binding buffer was added, followed by incubation for a further 30 min at room temperature. The resin was washed with 2 ml of binding buffer with 10 mM imidazole and eluted with 40 µl 4× sodium dodecyl sulfate (SDS)–PAGE sample buffer. Controls consisted of adding prey to resin without bait. All samples were run on SDS–PAGE and stained with Coomassie blue. Each experiment was replicated two times.

Glutathione pull-down assay

The bait proteins, MMACHC, $MMADHC^{\Delta N}$ or $MTRR^{\Delta FMN}$ each with a N-terminal GST-tag at 0.3 mg ml^{-1} were mixed with either prey proteins MTR^{FL}, $MTR^{N\text{-}Half}$ or $MTR^{C\text{-}Half}$ without GST-tags at 0.3 mg ml^{-1} in a total volume of 100 µl diluted in binding buffer (25 mM HEPES, pH 7.5, 100 mM NaCl, 1 mM TCEP, 0.2% Tween-20). Protein mixes were incubated with rotation at room temperature for 30 min. Next, 200 µl of a 50% slurry of glutathione sepharose 4 fast flow resin (Cytiva) in binding buffer was added, followed by incubation for a further 60 min at room temperature. The resin was washed with 2 ml of binding buffer and eluted with 40 µl 4× sodium dodecyl sulfate (SDS)–PAGE sample buffer. Controls consisted of adding prey to resin without bait. All samples were run on SDS–PAGE and stained with Coomassie blue. Each experiment was replicated two times.

Cobalamin loading assay

Cobalamin loading from MMADHC to MTR was carried out as similar to described[17]. 100 µM of HOCbl was mixed with 120 µM of $MMADHC^{\Delta N}$ in KCl Buffer (100 mM HEPES, 150 mM KCl, 10% glycerol) for a final volume of 40 µL. The reaction was incubated at room temperature for 1 hour, and the UV-Vis spectrum was recorded every 3 minutes to check the reaction. To detect the cobalamin transfer from $MMADHC^{\Delta N}$ to MTR^{FL}, $MMADHC^{\Delta N}$ bound was concentrated by multiple rounds of centrifugation (4000 xg, 4 °C) in Amicon® concentrators

with a 10 kDa molecular weight cut-off (Sigma Aldrich) followed by adding more KCl buffer to remove free HOCbl. 15 µM MMADHC$^{\Delta N}$ -HOCbl was then incubated with 8.8 µM of MTR in a final volume of 100 µL of KCl buffer for 1 hour at room temperature. After this time, the sample was loaded into a Superose® 6 10/300 GL gel filtration column (Cytiva) equilibrated with KCl buffer at 4 °C at a flow rate of 0.2 ml/min. The elution profile was monitored at 280 and 350 nm to detect the protein and cobalamin respectively. For binding of HOCbl and MeCbl, 8.8 µM of MTR^{FL} was incubated with 100 µM Cbl for and the applied onto the gel filtration column. All experiments were performed twice except for MeCbl binding which was carried out only once.

Analytical size exclusion chromatography

Analytical size exclusion chromatography was carried out using a 10/300 GL S200 Increase column (Cytiva) equilibrated in 25 mM HEPES, pH 7.5, 150 mM NaCl. Proteins were mixed as appropriate in 25 mM HEPES, pH 7.5, 150 mM NaCl to a final concentration of each protein at 1.5 mg/ml in a total volume of 250 ul. After 30 minutes incubation rotating at room temperature each were loaded onto the size-exclusion column and eluted with a flow rate of 0.3 ml/min. 500 µl fractions were collected for analysis by SDS-PAGE.

Data availability

The authors declare that the main data supporting the findings of this study are available within the article and Supplementary Information. EM maps and models generated in this study of Human Methionine Synthase With Methyltetrahydrofolate, N-Half From Full-Length (EMDB-55190, PDB 9SSP), Human Methionine Synthase With Methyltetrahydrofolate, C-Half From Full-Length (EMDB-55191, PDB 9SSQ), Human Methionine Synthase With Methyltetrahydrofolate, Hydroxocobalamin, and SAM, N-Half From Full-Length (EMDB-55192, PDB 9SSR), Human Methionine Synthase With Methyltetrahydrofolate, Hydroxocobalamin, and SAM, C-Half His-ON From Full-Length (EMDB-55193, PDB 9SSS), Human Methionine Synthase With Methyltetrahydrofolate, Hydroxocobalamin, and SAM, C-Half His-OFF From Full-Length (EMDB-55194, PDB 9SST), Human Methionine Synthase With Methylcobalamin, N-Half From Full-Length (EMDB-55195, PDB 9SSU) and Human Methionine Synthase With Methylcobalamin, Activation Domain From Full-Length (EMDB-55196, PDB 9SSV), have been deposited to the Electron Microscopy Data Bank (EMDB) and Protein Data Bank (PDB) Other structures referenced in this article are indicated, including PDB ID 8G3H, 8SSC, 9CBO, 9CBP, 9CBQ, and 9CBR. Source data are provided with this paper.

Acknowledgements

Negative stain electron microscopy was done at Newcastle University EM Research Services, and we are grateful to Tracey Davey for technical support. The Newcastle University EM Research Services is funded by the BBSRC (grant number BB/R013942/1). We thank Johan Turkenburg and Sam Hart for their assistance in collecting Glacios data at York Structural Biology Laboratory (YSBL). The YSBL is funded by the BBSRC, the Wellcome Trust (grant number 206161/Z/17/Z), Tony Wild, and the Wolfson Foundation. We acknowledge the Diamond Light Source for access and support to the UK's Electron Bio-imaging Centre (eBIC, under BAG proposal BI34172) funded by the Wellcome Trust, MRC, and BBRSC. We specifically want to thank David Owen and David Farmer for their assistance in data collecting. T.J.M. received cryo-EM training through the Wellcome/MRC funded programme (218785/Z/19/Z) The Structural Genomics Consortium is a registered charity (Number 1097737) that receives funds from AbbVie, Bayer Pharma AG, Boehringer Ingelheim, Canada Foundation for Innovation, Eshelman Institute for Innovation, Genome Canada, Innovative Medicines Initiative (EU/EFPIA) [ULTRA-DD grant no. 115766], Janssen, Merck & Co., Novartis Pharma AG, Ontario Ministry of Economic Development and Innovation, Pfizer, Sao Paulo Research Foundation-FAPESP, Takeda, and Wellcome Trust [092809/Z/10/Z]. W.W.Y. holds a visiting professorship at Nuffield Department of Medicine, University of Oxford.

Author contributions

D.S.M.F., J.M.E., J.A.C., W.W.Y., and T.J.M. designed the experiments. D.S.M.F. expressed and purified MTR and MTRR constructs, carried out biochemical experiments, screened, and collected EM data, analysed, and refined all cryo-EM structures. K.M., C.D., H.J.B., and J.K. purified MTR constructs and did preliminary experiments. W.K. expressed, purified, and crystallized the N-terminal MTR construct. M.V. solved and refined the N-terminal MTR construct crystal structure. D.S.F. expressed and purified MMADHC and MMACHC. T.J.M. expressed and purified MMACHC, MTRR and MTR proteins along with guiding cryo-EM screening, data collection, data processing, AF3 predictions, and biochemical experiments. R.C. carried out the native mass spectrometry. A.B. supplied computational resources for cryo-EM data processing. D.S.M.F., W.W.Y., and T.J.M. supervised the work, carried out data analysis, and wrote the manuscript with contributions from all authors.

Competing interests

The authors declare no competing interests.

Correspondence and requests for materials should be addressed to Wyatt W. Yue or Thomas J. McCorvie

References

1. Banerjee, R.V. & Matthews, R.G. Cobalamin-dependent methionine synthase. *The FASEB journal* **4**, 1450-1459 (1990).
2. Chiang, P.K. et al. S-Adenosylmethionine and methylation. *FASEB J* **10**, 471-80 (1996).
3. Ghergurovich, J.M. et al. Methionine synthase supports tumour tetrahydrofolate pools. *Nat Metab* **3**, 1512-1520 (2021).
4. Sullivan, M.R. et al. Methionine synthase is essential for cancer cell proliferation in physiological folate environments. *Nat Metab* **3**, 1500-1511 (2021).
5. Wright, A.J., Dainty, J.R. & Finglas, P.M. Folic acid metabolism in human subjects revisited: potential implications for proposed mandatory folic acid fortification in the UK. *Br J Nutr* **98**, 667-75 (2007).
6. Froese, D.S., Fowler, B. & Baumgartner, M.R. Vitamin B12, folate, and the methionine remethylation cycle—biochemistry, pathways, and regulation. *Journal of inherited metabolic disease* **42**, 673-685 (2019).
7. McCorvie, T.J., Ferreira, D., Yue, W.W. & Froese, D.S. The complex machinery of human cobalamin metabolism. *Journal of Inherited Metabolic Disease* **46**, 406-420 (2023).
8. Matthews, R.G., Koutmos, M. & Datta, S. Cobalamin-dependent and cobamide-dependent methyltransferases. *Current opinion in structural biology* **18**, 658-666 (2008).
9. Evans, J.C. et al. Structures of the N-terminal modules imply large domain motions during catalysis by methionine synthase. *Proceedings of the National Academy of Sciences* **101**, 3729-3736 (2004).
10. Bandarian, V. et al. Domain alternation switches B12-dependent methionine synthase to the activation conformation. *Nature structural biology* **9**, 53-56 (2002).
11. Drennan, C.L., Huang, S., Drummond, J.T., Matthews, R.G. & Ludwig, M.L. How a protein binds B12: a 3.0 Å X-ray structure of B12-binding domains of methionine synthase. *Science* **266**, 1669-1674 (1994).
12. Bassila, C. et al. Methionine synthase and methionine synthase reductase interact with MMACHC and with MMADHC. *Biochimica et Biophysica Acta (BBA)-Molecular Basis of Disease* **1863**, 103-112 (2017).
13. Froese, D.S. et al. Structure of MMACHC reveals an arginine-rich pocket and a domain-swapped dimer for its B12 processing function. *Biochemistry* **51**, 5083-5090 (2012).

14. Froese, D.S. et al. Structural insights into the MMACHC-MMADHC protein complex involved in vitamin B12 trafficking. *Journal of Biological Chemistry* **290**, 29167-29177 (2015).
15. Mascarenhas, R. et al. An unusual Co-S bond links B(12) chaperones in an interprotein complex. *Proc Natl Acad Sci U S A* **122**, e2507700122 (2025).
16. Li, Z. et al. An interprotein Co–S coordination complex in the B12-trafficking pathway. *Journal of the American Chemical Society* **142**, 16334-16345 (2020).
17. Mascarenhas, R. et al. Cobalt–Sulfur Coordination Chemistry Drives B12 Loading onto Methionine Synthase. *Journal of the American Chemical Society* **145**, 24678-24689 (2023).
18. Wolthers, K.R., Basran, J., Munro, A.W. & Scrutton, N.S. Molecular dissection of human methionine synthase reductase: determination of the flavin redox potentials in full-length enzyme and isolated flavin-binding domains. *Biochemistry* **42**, 3911-3920 (2003).
19. Wolthers, K.R. & Scrutton, N.S. Cobalamin uptake and reactivation occurs through specific protein interactions in the methionine synthase–methionine synthase reductase complex. *The FEBS Journal* **276**, 1942-1951 (2009).
20. Olteanu, H. & Banerjee, R. Human methionine synthase reductase, a soluble P-450 reductase-like dual flavoprotein, is sufficient for NADPH-dependent methionine synthase activation. *Journal of Biological Chemistry* **276**, 35558-35563 (2001).
21. Hall, D.A. et al. Mapping the interactions between flavodoxin and its physiological partners flavodoxin reductase and cobalamin-dependent methionine synthase. *Proc Natl Acad Sci U S A* **98**, 9521-6 (2001).
22. Froese, D.S. & Gravel, R.A. Genetic disorders of vitamin B12 metabolism: eight complementation groups–eight genes. *Expert reviews in molecular medicine* **12**, e37 (2010).
23. Copp, A.J., Stanier, P. & Greene, N.D. Neural tube defects: recent advances, unsolved questions, and controversies. *Lancet Neurol* **12**, 799-810 (2013).
24. Mendoza, J., Purchal, M., Yamada, K. & Koutmos, M. Structure of full-length cobalamin-dependent methionine synthase and cofactor loading captured in crystallo. *Nature Communications* **14**, 6365 (2023).
25. Yamada, K., Gravel, R.A., Toraya, T. & Matthews, R.G. Human methionine synthase reductase is a molecular chaperone for human methionine synthase. *Proceedings of the National Academy of Sciences* **103**, 9476-9481 (2006).
26. Drummond, J.T., Jarrett, J., Gonzalez, J.C., Huang, S. & Matthews, R.G. Characterization of nonradioactive assays for cobalamin-dependent and cobalamin-independent methionine synthase enzymes. *Analytical biochemistry* **228**, 323-329 (1995).
27. Watkins, M.B., Wang, H., Burnim, A. & Ando, N. Conformational switching and flexibility in cobalamin-dependent methionine synthase studied by small-angle X-ray scattering and cryoelectron microscopy. *Proceedings of the National Academy of Sciences* **120**, e2302531120 (2023).
28. Datta, S., Koutmos, M., Pattridge, K.A., Ludwig, M.L. & Matthews, R.G. A disulfide-stabilized conformer of methionine synthase reveals an unexpected role for the histidine ligand of the cobalamin cofactor. *Proceedings of the National Academy of Sciences* **105**, 4115-4120 (2008).
29. Koutmos, M., Datta, S., Pattridge, K.A., Smith, J.L. & Matthews, R.G. Insights into the reactivation of cobalamin-dependent methionine synthase. *Proceedings of the National Academy of Sciences* **106**, 18527-18532 (2009).
30. Punjani, A. & Fleet, D.J. 3D variability analysis: Resolving continuous flexibility and discrete heterogeneity from single particle cryo-EM. *J Struct Biol* **213**, 107702 (2021).
31. Fleischhacker, A.S. & Matthews, R.G. Ligand trans influence governs conformation in cobalamin-dependent methionine synthase. *Biochemistry* **46**, 12382-12392 (2007).

32. Jarrett, J.T., Huang, S. & Matthews, R.G. Methionine synthase exists in two distinct conformations that differ in reactivity toward methyltetrahydrofolate, adenosylmethionine, and flavodoxin. *Biochemistry* **37**, 5372-5382 (1998).
33. Mendoza, J., Yamada, K., Castillo, C., Wilhelm, C.A. & Koutmos, M. Orchestrating Improbable Chemistries: Structural Snapshots of B12-Dependent Methionine Synthase's Catalytic Choreography. *bioRxiv*, 2024.08.29.610163 (2024).
34. Wolthers, K.R. et al. Crystal structure and solution characterization of the activation domain of human methionine synthase. *The FEBS Journal* **274**, 738-750 (2007).
35. Fofou-Caillierez, M.a.B. et al. Interaction between methionine synthase isoforms and MMACHC: characterization in cblG-variant, cblG and cblC inherited causes of megaloblastic anaemia. *Human molecular genetics* **22**, 4591-4601 (2013).
36. Abramson, J. et al. Accurate structure prediction of biomolecular interactions with AlphaFold 3. *Nature*, 1-3 (2024).
37. Li, Z. et al. An Interprotein Co–S Coordination Complex in the B_{12}-Trafficking Pathway. (2020).
38. Wolthers, K.R. & Scrutton, N.S. Protein interactions in the human methionine synthase− methionine synthase reductase complex and implications for the mechanism of enzyme reactivation. *Biochemistry* **46**, 6696-6709 (2007).
39. Jarrett, J.T., Hoover, D.M., Ludwig, M.L. & Matthews, R.G. The mechanism of adenosylmethionine-dependent activation of methionine synthase: a rapid kinetic analysis of intermediates in reductive methylation of cob (II) alamin enzyme. *Biochemistry* **37**, 12649-12658 (1998).
40. Bandarian, V., Ludwig, M.L. & Matthews, R.G. Factors modulating conformational equilibria in large modular proteins: a case study with cobalamin-dependent methionine synthase. *Proceedings of the National Academy of Sciences* **100**, 8156-8163 (2003).
41. Banerjee, R.V., Frasca, V., Ballou, D.P. & Matthews, R.G. Participation of cob(I) alamin in the reaction catalyzed by methionine synthase from Escherichia coli: a steady-state and rapid reaction kinetic analysis. *Biochemistry* **29**, 11101-9 (1990).
42. Guha, A. & Banerjee, R. The common homocystinuria-associated P1173L variant of human methionine synthase impairs reductive methylation. *J Biol Chem* **301**, 110366 (2025).
43. Suormala, T. et al. The cblD defect causes either isolated or combined deficiency of methylcobalamin and adenosylcobalamin synthesis. *Journal of Biological Chemistry* **279**, 42742-42749 (2004).
44. Haque, M.M. et al. Distinct conformational behaviors of four mammalian dual-flavin reductases (cytochrome P450 reductase, methionine synthase reductase, neuronal nitric oxide synthase, endothelial nitric oxide synthase) determine their unique catalytic profiles. *FEBS J* **281**, 5325-40 (2014).
45. Punjani, A., Rubinstein, J.L., Fleet, D.J. & Brubaker, M.A. cryoSPARC: algorithms for rapid unsupervised cryo-EM structure determination. *Nature methods* **14**, 290-296 (2017).
46. Bepler, T. et al. Positive-unlabeled convolutional neural networks for particle picking in cryo-electron micrographs. *Nat Methods* **16**, 1153-1160 (2019).
47. Varadi, M. et al. AlphaFold Protein Structure Database: massively expanding the structural coverage of protein-sequence space with high-accuracy models. *Nucleic Acids Res* **50**, D439-D444 (2022).
48. Pettersen, E.F. et al. UCSF ChimeraX: Structure visualization for researchers, educators, and developers. *Protein science* **30**, 70-82 (2021).
49. Croll, T.I. ISOLDE: a physically realistic environment for model building into low-resolution electron-density maps. *Acta Crystallographica Section D: Structural Biology* **74**, 519-530 (2018).
50. Terwilliger, T.C. et al. Iterative model building, structure refinement and density modification with the PHENIX AutoBuild wizard. *Acta Crystallographica Section D: Biological Crystallography* **64**, 61-69 (2008).

1127 51. Emsley, P. & Cowtan, K. Coot: model-building tools for molecular graphics. *Acta*
1128 *Crystallogr D Biol Crystallogr* **60**, 2126-32 (2004).
1129 52. Moriarty, N.W., Grosse-Kunstleve, R.W. & Adams, P.D. electronic Ligand Builder and
1130 Optimization Workbench (eLBOW): a tool for ligand coordinate and restraint
1131 generation. *Acta Crystallogr D Biol Crystallogr* **65**, 1074-80 (2009).
1132 53. Chen, V.B. et al. MolProbity: all-atom structure validation for macromolecular
1133 crystallography. *Acta Crystallogr D Biol Crystallogr* **66**, 12-21 (2010).
1134 54. Pintilie, G. et al. Measurement of atom resolvability in cryo-EM maps with Q-scores.
1135 *Nat Methods* **17**, 328-334 (2020).
1136 55. Jumper, J. et al. Highly accurate protein structure prediction with AlphaFold. *Nature*
1137 **596**, 583-589 (2021).
1138 56. Zhang, Y. & Skolnick, J. Scoring function for automated assessment of protein
1139 structure template quality. *Proteins* **57**, 702-10 (2004).
1140 57. Xu, J. & Zhang, Y. How significant is a protein structure similarity with TM-score = 0.5?
1141 *Bioinformatics* **26**, 889-95 (2010).
1142